

JUACEP Program 2019

at UCLA & University of Toronto



Japan-US-Canada Advanced Collaborative Education Program

Nagoya University

Table of Contents

<1> About the Program	
(a) Overview.....	3
(b) Participants.....	4
(c) Schedule.....	5
<2> Research Reports.....	7
<3> Research Presentations	
● The 26 th JUACEP Students Workshop	35
<4> Findings through JUACEP	
● Students' reviews	49
● Questionnaires (in Japanese).....	57

<1> About the Program

(a) Overview ...3

(b) Participants ...4

(c) Schedule ...5

(a) Overview

JUACEP has provided three program courses for students of the Graduate School of Engineering at Nagoya University to study abroad: a short-term (two months) course; a medium-term (six months) course; a long-term (eight months) course. Choosing one of those courses the selected students are offered an opportunity to work together with faculty and other researchers or students from all over the world at the world's top universities.

Each student works on a research project related to his own master's thesis topic while belonging to a specialized research group of the University of Michigan (UM), UCLA or University of Toronto (UT). In addition to research implementation, the students are expected to attend the group seminars, the group discussions and other events. At the end of each course, the students are required to submit research reports to their mentors at the host institution, and after returning to Nagoya, give research presentations based on their achievements in front of the faculty and peer students at JUACEP Workshop held in Nagoya University. The report and the presentation are primary requisites to be accredited for the program completion.

This publication is compiling the activities of the following students.

[a] Six students of medium-term course from August 2019 to January 2020 at UCLA

[b] One student of medium-term course from August 2019 to January 2020 at UT

[c] One student of long-term course from August 2019 to March 2020 at UCLA

*There was no short-term course participant in 2019.

JUACEP 2019 Medium- and Long-term Courses Flowchart

	Medium-term course	Long-term course
January 2019	Public announcement and accepting application (Jan. - Mar.)	
February		
March		
April	Screening candidates	
May	Selected students approach the partner universities faculty to get post of 'Visiting Scholar' (called *VGR at UCLA and **IVGS at UT). After acceptance by faculty, visa procedure starts including examination of CV, English proficiency and other qualification.	
June		
July	US J-1 Visa or Canada Student Permit application	
August	[a, b] Medium-term course study at UCLA/UT Aug. 2019 – Jan. 2020	[c] Long-term course study at UCLA Aug. 2019 - Mar. 2020
September		
October		
November		
December		
January 2019		
February		
March	26 th Workshop, Mar. 26, 2020	
April		Presentation, Apr. 17, 2020

*VGR: Visiting Graduate Researcher for UCLA

**IVGS: International Visiting Graduate Students

(b) 2019 Participants

★Medium-term course at UCLA

August 1, 2019 - January 31, 2020

Keita Umemura 梅村 佳汰	M1	Assoc.Prof. Kazuhiro Yamamoto Mechanical Systems Engineering	Prof. Rajit Gadh Mechanical and Aerospace Engineering
------------------------	----	---	--

August 7, 2019 - January 31, 2020

Takumi Kani 蟹 拓実	M1	Prof. Noritsugu Umehara Micro-Nano Mechanical Science and Engineering	Prof. Laurent Pilon Mechanical and Aerospace Engineering
---------------------	----	---	---

Yusaku Kawagoe 川越 悠作	M1	Prof. Toshiro Matsumoto Mechanical Systems Engineering	Prof. Aaswath Raman Materials Science and Engineering
-------------------------	----	---	--

Tomokohiro Saso 佐宗 朋洋	M1	Prof. Noritsugu Umehara Micro-Nano Mechanical Science and Engineering	Prof. Xiaochun Li Mechanical and Aerospace Engineering
--------------------------	----	---	---

Takeshi Matsumoto 松本 壮史	M1	Prof. Tsuyoshi Inoue Mechanical Systems Engineering	Prof. Tetsuya Iwasaki Mechanical and Aerospace Engineering
----------------------------	----	--	---

Tomoyasu Watanabe 渡邊 智康	M1	Prof. Noritsugu Umehara Micro-Nano Mechanical Science and Engineering	Prof. Suneel Kodambaka Materials Science and Engineering
----------------------------	----	---	---

★Medium-term course at University of Toronto

August 7, 2019 - January 31, 2020

Takaaki Mlyachi 宮地 孝明	M1	Prof. Noritsugu Umehara Micro-Nano Mechanical Science and Engineering	Prof. Shaker Meguid Mechanical and Industrial Engineering
--------------------------	----	---	--

★Long-term course at UCLA

August 7, 2019 - March 202, 2020

Masahiro Itoh 伊藤 正浩	M1	Prof. Koji Nagata Aerospace Engineering	Prof. Chang-Jin Kim Mechanical and Aerospace Engineering
------------------------	----	--	---

Coordinators at Partner Universities

Prof. Jenn-Ming Yang	Materials Science and Engineering
Prof. Shaker Meguid	Mechanical and Industrial Engineering

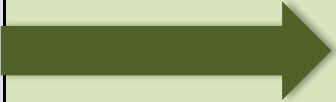
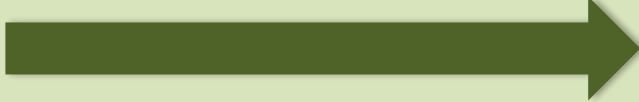
JUACEP Members

Prof. Yang Ju	Micro-Nano Mechanical Science and Engineering
Prof. Noritsugu Umehara	Micro-Nano Mechanical Science and Engineering
Prof. Toshiro Matsumoto	Mechanical Systems Engineering
Assoc. Prof. Yasumasa Ito	Mechanical Systems Engineering
Assoc. Prof. Takayuki Tokoroyama	Micro-Nano Mechanical Science and Engineering
Tomoko Kato, Administrative staff	JUACEP Office

JUACEP Office

Room #341, Engineering Building 2, Nagoya University
Furo-cho, Chikusa-ku, Nagoya 4648603 Tel/Fax +81 (0)52 789 2799

(c) JUACEP Research Abroad 2019 Schedule

Period	Medium-term course	Long-term course
2019/07/30~2019/08/06	Departure from Japan and starting of research activity at UCLA and Univ. Toronto	
2019/09	<div style="display: flex; justify-content: space-between; align-items: center;"> <div style="width: 45%;"> <p>Research activity at each lab</p>  </div> <div style="width: 45%;"> <p>Research activity at each lab</p>  </div> </div>	
2019/10		
2019/11		
2019/12		
2020/01		
2020/01/31~2020/02/03	Departure from US and arrival at Nagoya. Submission of Research report, JUACEP report, JASSO questionnaire and evaluation sheet to JUACEP Office.	
2020/02	<div style="display: flex; justify-content: space-between; align-items: center;"> <div style="width: 45%;"></div> <div style="width: 45%;"> <p>Departure from US and arrival at Nagoya. Submission of Research report, JUACEP report, JASSO questionnaire and evaluation sheet to JUACEP Office.</p> </div> </div>	
2020/03		
2020/03/22		
2020/03/26	26th Workshop, Presentations for Medium-term Course	
2020/4/17	Presentation for Long-term Course	

<2> Research Reports

Studies at UCLA

- [L] Masahiro Itoh, *mentored by Prof. Chang-Jin Kim* ...P.9
“The Wind Tunnel Experiment of Low Profile Double Floating-Elements Shear Stress Sensor”
- [M] Keita Umemura, *mentored by Prof. Rajit Gadh* ...P.14
“About ISO 15118”
- [M] Takumi Kani, *mentored by Prof. Laurent Pilon* ...P.20
“Development of Low Adhesion Film Using Mesoporous Silica”
- [M] Yusaku Kawagoe, *mentored by Prof. Aaswath Raman* ...P.25
“Conditional Machine Learning-Based Inverse Design of Photonic Metasurfaces”
(*Undisclosed*)
- [M] Tomohiro Saso, *mentored by Prof. Xiaochun Li* ...P.26
“Study of Tribological Performance of Aluminum Alloy 7075(T6)-TiB₂ Nanocomposites”
(*Undisclosed*)
- [M] Takeshi Matsumoto, *mentored by Prof. Tetsuya Iwasaki* ...P.27
“Toward Robust Tuning of Integral Resonant Control”
(*Undisclosed*)
- [M] Tomoyasu Watanabe, *mentored by Prof. Suneel Kodambaka* ...P.28
“Effects of Pulse Width of VNbTaMoW High Entropy Alloy Thin Films Deposited by HiPIMS”
(*Undisclosed*)

Study at University of Toronto

- [M] Takaaki Miyachi, *mentored by Prof. Shaker A. Meguid* ...P.29
“Finite Element Analysis of Contact in Asperities”

[M] Medium-term course; [L] Long-term course

THE WIND TUNNEL EXPERIMENT OF LOW PROFILE DOUBLE FLOATING-ELEMENTS SHEAR STRESS SENSOR

Masahiro Itoh

Department of Aerospace Engineering, Graduate School of Engineering, Nagoya University
itoh.masahiro@a.mbox.nagoya-u.ac.jp

Chang-Jin Kim

Department of Mechanical and Aerospace Engineering, University of California, Los Angeles
cjkim@ucla.edu

ABSTRACT

Measuring shear stress of airflow is challenging attempt in fluid dynamics. Using a floating-element shear stress sensor originally developed for shear stress sensing of liquid flows^[1], in this study, I evaluated the sensor for wind tunnel experiments. The sensor has two floating elements, and shear stress on the surface of samples mounted on the floating elements is directly measured simultaneously. Experiments were performed first with two smooth samples on the two floating elements and then with one smooth sample and one riblet sample on the two floating elements, both at 5~40m/s. At velocity lower than 20m/s, shear stress was too small and could not be accurately measured. At 20~40m/s, the sensor worked well. The result confirmed the given sensor can measure shear stress on surface samples accurately for airflow.

1.Introduction

Shear stress is generated at wall when fluid flows on the surface of object by velocity gradient between fluid and the surface of object. Measuring shear stress accurately is important for friction drag evaluation of transportation equipment, for example vehicle and aircraft.

There are two kinds of measuring shear stress methods. The first method is indirect method. In this method, shear stress is measured from other flow properties that are related to shear stress. For instance, hot-film shear stress sensor measures temperature at wall and convert it to shear stress by using other flow properties. The advantage is high reactivity, high sensitivity and that the sensor is small. The disadvantage is low accuracy because this need to use assumption to get the shear stress value. The second method is direct method. In this method, shear stress is measured directly. For instance, floating element sensor measures displacement of floating element. The advantage is high accuracy because the sensor measures shear stress directly and assumption is not needed. The disadvantage is that the sensor is bulky and that structure is complex. In Professor CJ Kim's lab at UCLA, a direct shear sensor with double floating elements that is also compact and of low profile has been developed for hydrodynamic applications^[1]. A previous JUACEP student showed the same shear sensor can be used for aerodynamic flows in a wind

tunnel. In this study, I confirm the previous results and further characterize the sensor in air flows.

2. Mechanism and assembly

2.1 Mechanism

The sensor is assembled by multiple plates and sheets, as shown in Fig.1. This sensor allows us to compare the shear stresses on two surface different type samples placed side-by-side in a flow. The sensor plate has two floating elements which is suspended by flexure beam as shown in Fig.1 and Fig.2. The floating element can move only in the direction of airflow. The sensor plates fit into the circular plate, which is, in turn, fits onto the inner wall of the wind tunnel. The encoder plate has two optical encoders (M2000 linear encoder, Celera Motion Inc.) which have 78nm resolution. The optical scale is attached to the back side of each of the two floating elements, and the optical encoder senses the absence or presence of light on the optical scale and measure displacement of the floating element. Holding sheets are attached on the floating elements and the surface samples are mounted on the holding plate. The samples are made of silicon wafer. The cover sheet is to level the surface of the sensor with the surface of the samples. Shear stress is calculated with spring constant of beam, the sample displacement and sample size.

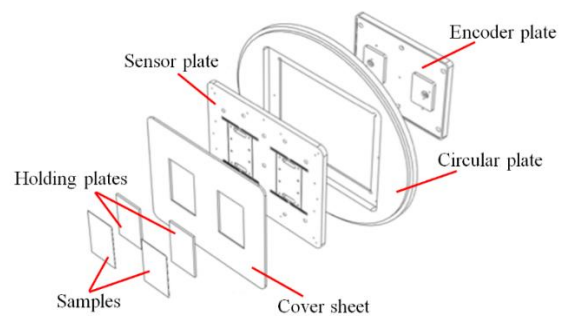


Fig.1 Structure of the sensor

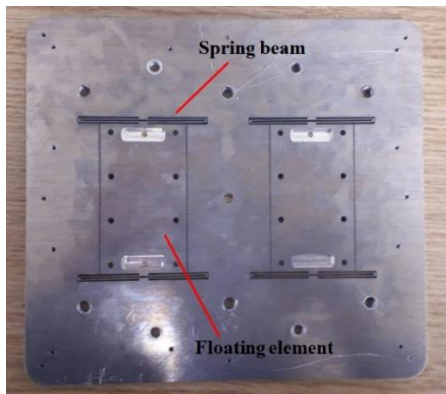


Fig.2 The sensor plate

2.2 Assembly

Most parts are assembled with mechanical screws to allow adjustments as well as repeated assemblies and disassembles. The height difference between the surface of the cover sheet and the surface of the circular plate at the front edge of the cover sheet needs to be removed in order to make the sensor plate flat for less effect to airflow. Also, because the cover sheet is thin, I needed to put some spacers between the sensor plate and the cover sheet and screw the cover sheet on the sensor plate at point a, b and c (on the edge of the cover sheet) as shown in Fig.3 to minimize steps, i.e., the height differences between surfaces. Because there are lots of thickness spacers, I choose some of them with considering total thickness in order to make the height difference $0\mu\text{m}$. There are designed gaps between the sample and cover sheet so that the samples can vibrate in the direction of airflow. The height difference and the gap are measured by microscope.

The displacement of the sample is affected by the height difference between the sample and the cover sheet. When the height of the sample surface is over $5\mu\text{m}$ higher than the cover sheet surface, shear stress that the sensor measured increases and the displacement of the sample increases. When the height of the sample surface is over $10\mu\text{m}$ lower than the cover sheet surface, shear stress that the sensor measured decreases and the displacement of the sample decreases. The height of the sample surface needs to be less than $5\mu\text{m}$ lower than that of the cover sheet surface. I need to put some spacers between the sensor plate and the holding plate and screw the holding plate on the sensor plate (sample is mounted on the holding plate) at point d, e, f and g (the four corners of the sample) as shown in Fig.3 for adjusting the height difference of these. I choose some of the spacers with considering total thickness likewise. When adjusting the height of the sample, I need to see the cover sheet surface and the sample surface by microscope simultaneously. If the floating element is vibrating at this time, the surface of the sample can't be seen clearly. Therefore, the floating element should be fixed with cover sheet by adhesive tape on back side of them. At this time, the sensor should be parallel to the ground because floating element should be fixed so that spring beam of it is equilibrium mode distribution. I checked how much displacement the floating element move at 40m/s (maximum air speed in the experiment). These are $41\mu\text{m}$ at front gap and $59\mu\text{m}$ at rear gap. Also, there are designed gap between the both side of the sample and the cover sheet. To make enough

gap, I put some ribbon spacers at front, rear, side of the sample.

Following are the steps to install the samples on the sensor.

1. Attach adhesive tape on back side of cover sheet and fix floating element on it. (Fig.4)
2. Put some vinyl ribbon spacers on 4 edges of the space for the sample (Fig.5).
3. Put some spacers between the sensor plate and the holding plate (the sample is mounted on the holding plate) (Fig.6).
4. Put the sample on the sensor plate. (Fig.7)
5. Screw the holding plate on the sensor plate.
6. Measure the height difference between the surface of the sample and that of the cover sheet.
7. In order to make the height of the sample surface less than $5\mu\text{m}$ lower than that of the cover sheet surface, repeat the steps 2~6.

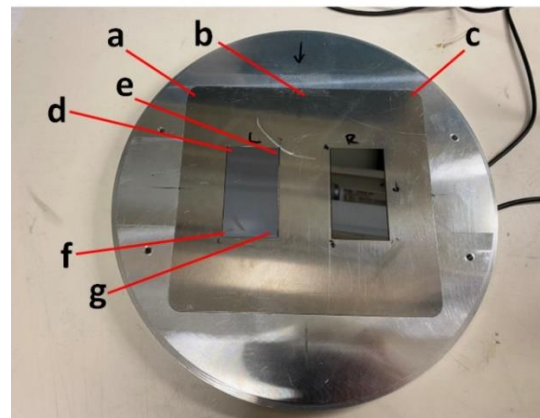


Fig.3 The sensor



Fig.4 Adhesive tape

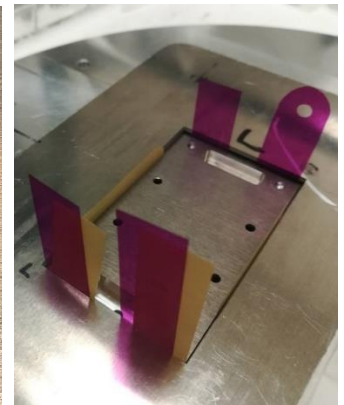


Fig.5 The ribbon spacers



Fig.6 The spacers

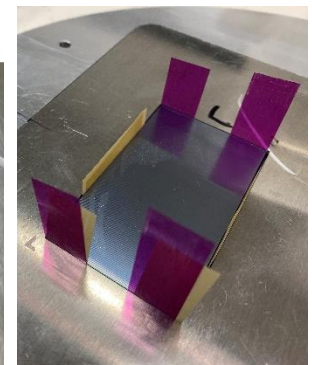


Fig.7 The sample

3. Experiment

3.1 The wind tunnel

The wind tunnel I used for experiment is Educational Wind Tunnel (AEROLAB) with a 12"x12"x24", i.e., 30.5cm x 30.5cm x 61cm, test section, as shown in Fig.4 and Fig.5. The speed of airflow is typically determined with a Pitot-static probe. For wind tunnel testing, however, a permanently-mounted probe is inconvenient. To eliminate the need for a probe, test section static pressure is sensed through holes drilled into the walls of the test section entrance (one pressure orifice in the middle of each surface). These holes are then plumbed together to form a manifold termed a static pressure "ring". This ring provides the average static pressure of the undisturbed flow at that location – also termed "test section static pressure". For airspeed calculations, atmospheric pressure is assumed to be the wind tunnel total pressure. This is a good assumption, but not completely accurate. There are very small pressure losses as the flow passes through the honeycomb, screens and ducting. The difference between atmospheric pressure and the test section static ring pressure is then assumed to be dynamic pressure "q". Assuming, also, standard sea level pressure, airspeed is from Bernoulli's equation.

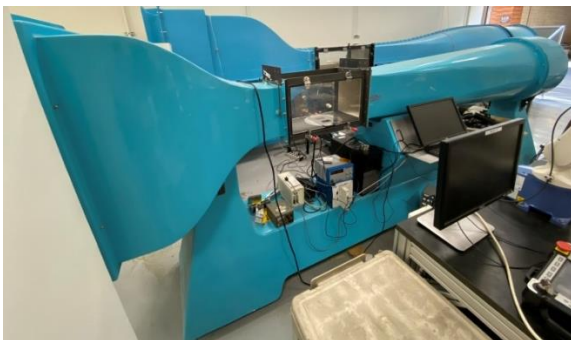


Fig.8 The wind tunnel

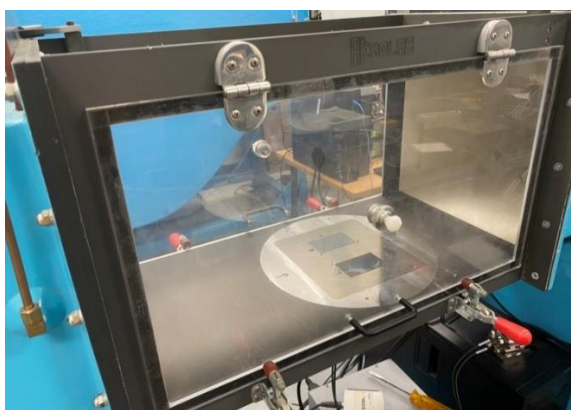


Fig.9 The test section

3.2 Samples

Two types of surface sample were used in this research. One is a reference sample with smooth surface. Another one is a target sample with blade-type riblets as shown in Fig.10. Riblet is a structure with regular groove which was inspired by shark skin, bird's feather and so on. Many types of riblets have been studied, and previous studies have shown that blade riblet would gain the highest drag reduction compared with any other types of riblets tested so far. Both the smooth

sample and the riblet sample are made of silicon, and the riblet sample is fabricated using MEMS fabrication technology. I adjusted the sheets to make the top of riblets (as shown in Fig.10) are less than 5 μ m lower than that of the cover sheet surface.

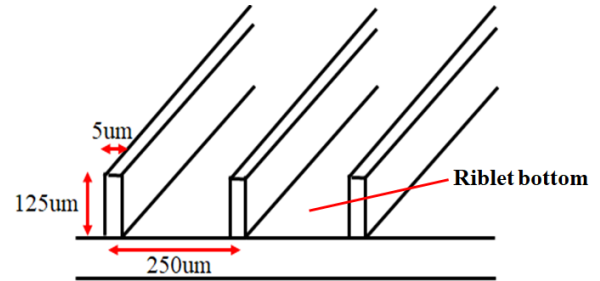


Fig.10 Dimension of the riblet

4. Experiment result

This sensor measures the average of shear stress. The sensor gets 10000 displacement data while vibrating. The interval time between each displacement data is 1.95ms. The wind velocity I experimented are every 5m/s from 5m/s to 30m/s and every 2.5m/s from 30m/s to 40m/s. Experiment is repeated 4 times. The displacement data at 0m/s is measured and the average of the displacement is calculated. The experiment was done up to the laminar-turbulent transition range in terms of Reynolds number.

4.1 Experiment with two smooth surfaces

I experimented with two smooth surfaces to check the error of drag reduction rate between them. The error of drag reduction shear stress at the velocity lower than 20m/s are 8.8% at 5m/s, 38.4% at 10m/s and 10.9% at 15m/s (values are the average of 4 data). The reason why the error is big is because the displacement is so small that it is much affected by vibration of the sample. Therefore, I put the error at 20~40m/s on Fig.12. As shown in Fig.12, the average of 4 shear stress error between left and right sample at 20~40 m/s are 0.5~2.6%. A previous JUACEP student also experimented with two smooth surfaces. In Fig.13, the average of shear stress error of this study and the previous study are plotted together for comparison. Shear stress error of previous study is -2.1~2.9%, confirming the repeatability of the shear stress error.

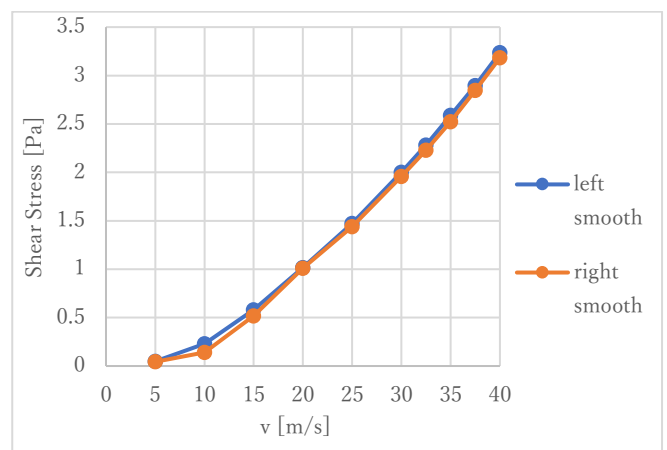


Fig.11 Shear stress at 5~40m/s

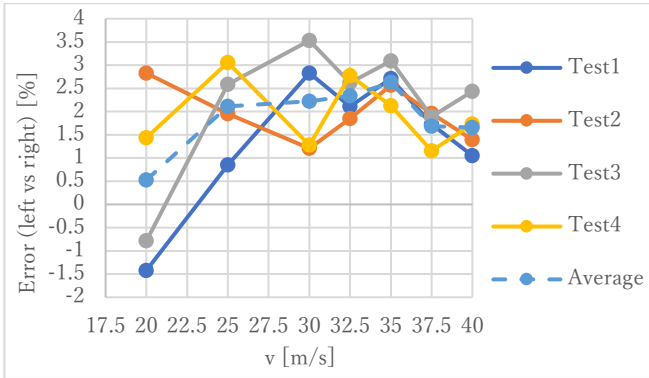


Fig.12 Shear stress error (Left vs Right) at 20~40m/s

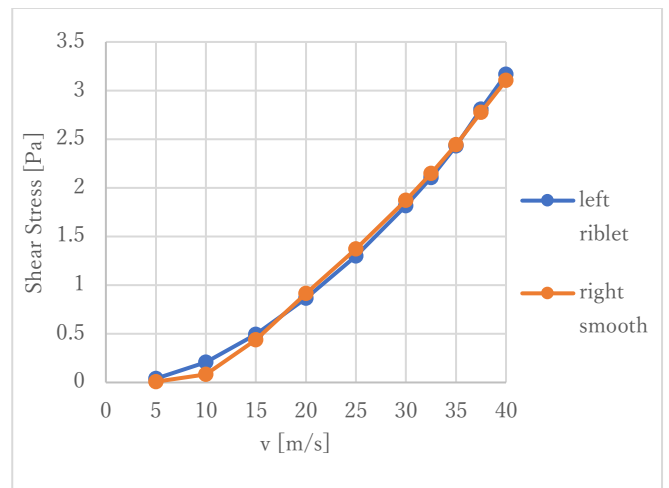


Fig.15 Shear stress at 5~40m/s

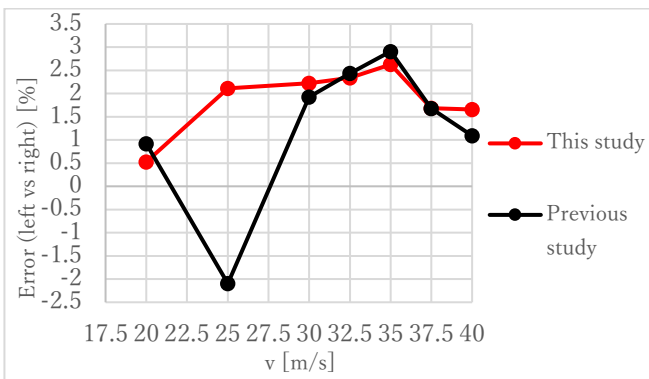


Fig.13 Shear stress error (Left vs Right) at 20~40m/s between this study and previous study

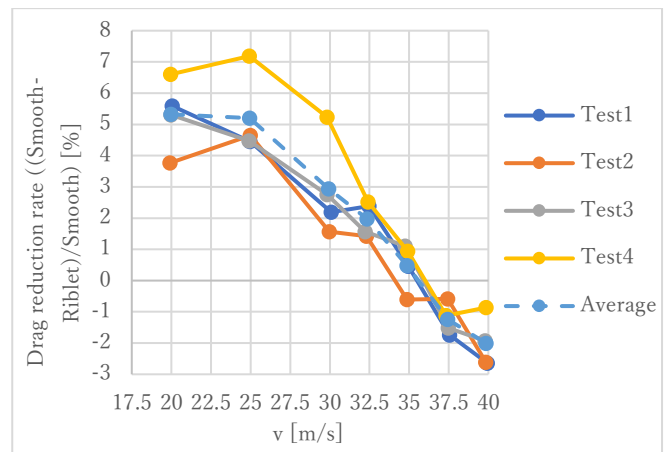


Fig.16 Drag reduction rate ((Smooth-Riblet)/Smooth) at 20~40m/s

4.2 Experiment with a smooth surface and a riblet surface

I experimented with a smooth surface and a riblet surface to check drag reduction rate of riblet surface. Before I experimented, I unintentionally damaged to the riblet surface. As I mentioned in section 4.1, I put the error at 20~40m/s on Fig.16. As shown in Fig.16, the average of 4 drag reduction rate by using riblet surface is -2.0~5.3%. The average of 4 drag reduction rate is highest (5.3%) at 20m/s and decrease as velocity is big. A previous JUACEP student also experimented with a smooth surface and the same blade riblet surface used in this study. As shown in Fig.17, the maximum drag reduction rate was 9.5% at 20m/s in the previous study. The drag reduction in this study was less than that of the previous study most likely because the riblet surface was damaged.

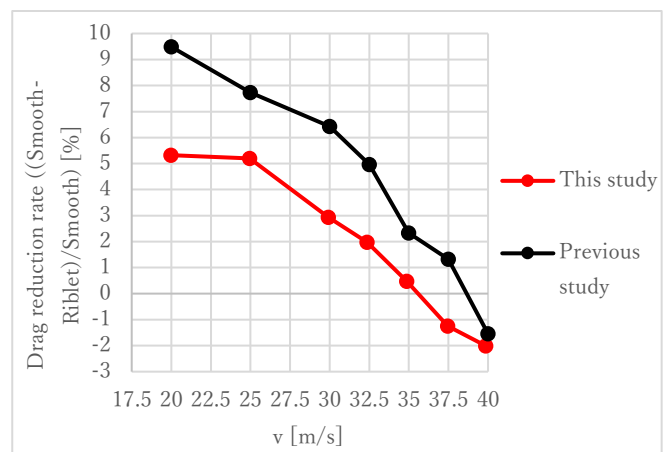


Fig.17 Drag reduction rate ((Smooth-Riblet)/Smooth) at 20~40m/s between this study and previous study

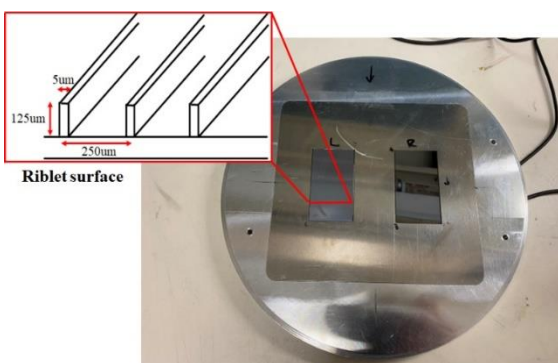


Fig.14 Smooth and riblet samples

5. Summary

In this study, I characterized the shear sensor and obtained results consistent with the preliminary study by the previous JUACEP student. I measured shear stress by using floating element sensor in the wind tunnel. The sensor worked well in the wind tunnel at 20~40m/s but couldn't measure shear

stress accurately under 20m/s because the displacement at these velocities is too small and significantly affected by vibration of the sample. The experiment with two smooth surface samples in this experiment shows the shear stress error between these samples are 0.5~2.6%. Considering that that of previous study is -2.1~2.9%, repeatability of the shear stress error was confirmed. The experiment with the smooth surface sample and the blade riblet surface sample in this study shows the drag reduction rate by using riblet surface is -2.0~5.3% and is highest (5.3%) at 20m/s. Because of the damage on the riblet surface, drag reduction rate of this study is smaller than that of the previous study. However, the highest drag reduction rate was at the velocity of 20m/s in both studies, and the drag reduction rate decreased with velocity in both studies. These result shows the sensor can be

used for aerodynamics experiments and confirmed the drag reducing capability of riblet sample.

REFERENCES

[1] Xu, M., Arihara, B., Tong, H. et al. A low-profile wall shear comparator to mount and test surface samples. *Exp Fluids* 61, 82 (2020).

Acknowledgements

I appreciate to Dr. Chang-Jin Kim, Professor of University of California, Los Angeles for accepting me as visiting student and advising me a lot and my labmates for helping me. I also appreciate to JUACEP program for giving me such a great opportunity.

ABOUT ISO 15118

Umemura Keita

Mechanical and Aerospace Engineering, Graduate School of UCLA
umemura.keita@h.mbox.nagoya-u.ac.jp

Supervisor: Rajit Gadh

Mechanical and Aerospace Engineering, Graduate School of UCLA
gadh@ucla.edu

ABSTRACT

The pending energy crisis and the necessity to reduce green house gas emissions have led developing vehicles partly or completely propelled by electric energy. Much of the standardization work on dimensional and electrical specifications of the charging infrastructure and vehicle interface is already treated in the relevant ISO or IEC group. However, the question of information transfer between the vehicle, the local installation and the grid has not been treated sufficiently. ISO 15118 is the standard that governs the communication between EVCC that is within the EV and SECC that is within the EVSE, i.e., the charger. Vehicle to Grid Communication system consists of ISO 15118-1, -2, and -3. The first one includes general information and use-case definition. The second one does network and application protocol requirements. The last one does physical layer and Data link layer requirements.

SYMBOLS AND ABBREVIATED TERMS

ISO --the International Organization for Standardization
IEC --the International Electrotechnical Commission
EV --Electric Vehicle
EVCC --Electric Vehicle Communication Controller
SECC --Supply Equipment Communication Controller
EVSE --EV Supply Equipment
PWM --Public Width Modulation
OEM --Original Equipment Manufacturer
SA --Secondary Actor
HMI --Human Machine Interface
SOC --State of Charge
V2G --Vehicle to Grid
BEV --Battery Electric Vehicle
PHEV --Plug-in Hybrid Electric Vehicles
XML --Extensible Markup Language

EXI --Efficient XML Interchange
V2GTP --V2G Transfer Protocol
TLS --Transport Layer Security
TCP --Transmission Control Protocol
SDP --SECC Discovery Protocol
IPv6 --Internet Protocol Version 6
SLAC --Signal Level Attenuation Characterization
HLC --High Level Communication
HLE --Higher Layers Entities
OSI --Open Systems Interconnection

1. INTRODUCTION

ISO 15118 is the standard that governs the communication between EVCC that is within the EV and SECC that is within the EVSE, i.e., the charger. ISO 15118 can provide ease of payment, high security, supports V2G and AC and DC charging and inductive charging, optimal use of energy resources. Vehicle to Grid Communication document overview is shown in Fig. 1. ISO 15118 consists of the following parts, under the general title Road vehicles – Vehicle to grid communication interface;

- Part 1: General information and use-case definition
- Part 2: Network and application protocol requirements
- Part 3: Physical and data link layer requirements

The characteristic of each parts are described in this paper.

Primary actors are directly involved in the charging process. The information flow between EVCC and the SECC shall be specified according to all layers of the OSI.

2.1.3 CHARGING STEPS

The charging step are divided into 8 steps.

1. Start of charging process
 - Connect cable between EV and EVSE.
 - EVSE sends PWM duty cycle that is interpreted by EV.
2. Communication setup
 - EVCC sends first high level signal to SECC.
3. Certificate Handling
 - Replace invalid/expired certificate with new certificate from SA.
 - EVCC requests update providing SA info.
 - SECC asks SA for certificate update.
 - SECC updates certificate in EV.
 - If no certificate, EV identified with OEM provisioning certificate installed during EV production.
 - SECC can send certificate to all possible SA to obtain required certificate.
 - ISO 15118 does not specify requirements to pay by card/cash.
4. Identification, Authentication and Authorization
 - EVCC triggers initialization of authorization.
 - SECC and EVCC exchange ID(EVSE ID and Contract ID).
 - Both IDs maybe forwarded to SA for validation.
 - User could also type in some ID in HMI on EVSE which maybe sent to SA.
 - Session ID defined and process can start (charge/discharge/other).
5. Target setting and charge scheduling
 - SECC and EVCC exchange max current limitations.
 - If user inputs min SOC required at departure – SA can propose charging schedule to SECC based on power limits, local generation, sales tariff table etc. or SA sends information to SECC and then either SECC or EVCC generates schedule.
 - In case of DC charging, max possible power is sent.
6. Charge controlling and Re-scheduling
 - EVCC sends SECC the current status.
 - EVCC signs meter information from SECC.
 - SECC sends signed meter info to SA.

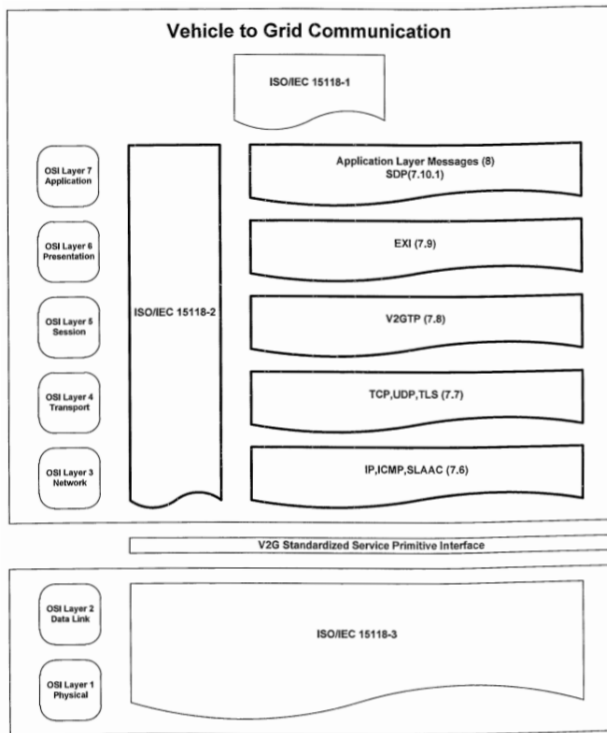


Fig. 1 Vehicle to Grid Communication document overview

2. ABOUT ISO 15118

2.1 ISO 15118-1

2.1.1 REQUIREMENTS

The requirements of ISO 15118-1 form the basic framework for all use cases descriptions and related documents in the ISO 15118 series. Communication in the context of this standard could be divided into two concepts called “basic signalling” and High Level Communication. High Level Communication is used to enable features like identification, payment, load levelling and value-added services. In case of AC charging, the EV performs the charging control itself. In case of DC charging, the charger located in the EVSE performs the charging control. And information exchange with HLC only occurs if both EV and EVSE are equipped with HLC device.

2.1.2 ACTORS

Fig. 2 shows all primary and secondary actors as well as their trigger functions that may be involved directly or indirectly in the charging procedure of ISO 15118.

- Charge rescheduling occurs if changes in info from SA (like local load change). SECC interrupts schedule and new schedule based on 5th.
- Charge reschedule also if user changes departure time or energy required.
- Reactive power compensation
 - EVCC indicates reactive power compensation is possible.
 - SECC requests reactive power compensation of certain value.
- V2G support
 - EVCC indicates V2G possibility, max rate of power discharge and energy given considering user constraints.
 - SECC requests V2G and provides grid schedule which EVCC can accept/reject.

7. Value-added services

- User requests information like pre-booking chargers, estimating energy required for journey etc., this I s sent from the SECC to the EVCC.
- Battery status and state of charging can be provided to SECC or SA from EVCC. EVCC can decline.

8. End of charging process

- User can request end of charging process on EV or EVSE side. Hence, EVCC will request SECC to stop charging or SECC directly stops.

2.2 ISO 15118-2

2.2.1 WHAT ISO 15118-2 DO?

- Specify the communication between BEV or PHEV and EVSE.
- Define messages, data model, XML/EXI based data representation format, usage of V2GTO, TLS, TCP and IPv6.

2.2.2 V2G COMMUNICATION STATES AND DATA LINK HANDLING

Fig. 2 depicts the general communication states of the V2G communication from an EVCC perspective.

[V2G2-014] - After data link layer connection is established, the EVCC shall start the IP address assignment mechanism.

[V2G2-018] - After that, EVCC start the process for discovering the SECC address.

[V2G2-021] - If the EV decides to apply a secured connection, the EVCC shall establish the Transport Layer Security connection to the SECC.

[V2G2-646] – If apply to unsecured connection, EVCC establish the Transmission Control Protocol connection to the SECC. Then TCP or TLS connection is established.

[V2G2-024] – The EVCC shall start the V2G Communication Session.

[V2G2-025] – EVCC terminate the TLS or TCP connection after stopping the V2G Communication..

[V2G2-717,718,720] – If the EVCC sent the session stop request, it terminate the data link, pause request, it pause the data link. If there are any error, it indicate an Data Link error and continue from the start point.

[V2G2-017,020,023] – When a certain time has passed, EVCC shall stop this all mechanism.

[V2G2-719] – If there are no link, whenever the EVCC receives the message about Data link ready, EVCC start this mechanism.

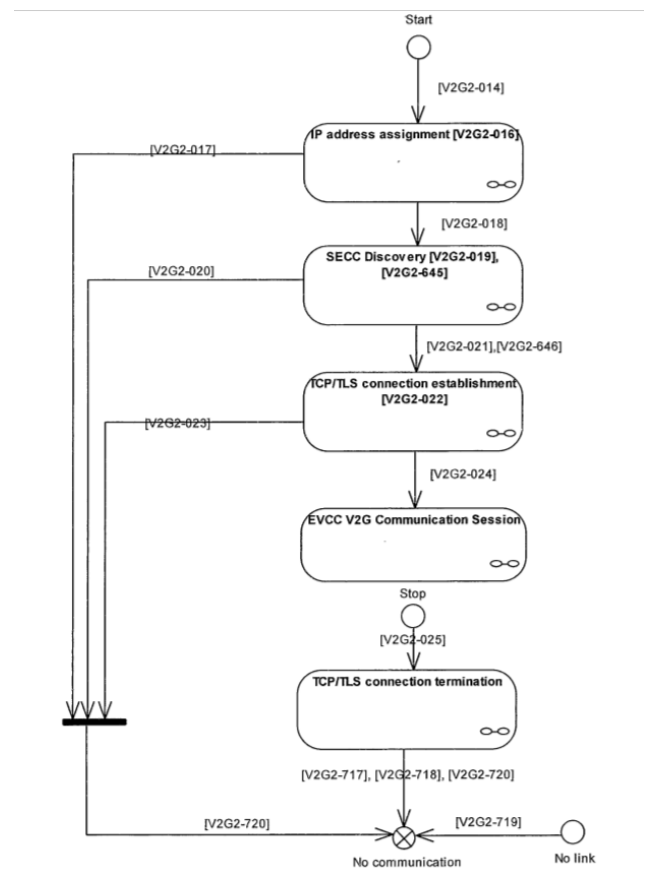


Fig. 2 Overview V2G Communication Session Status EVCC

Fig. 3 depicts the general communication states of the V2G communication from an SECC perspective.

[V2G2-721] – After successful data link establishment, SECC start the address assignment mechanism.

[V2G2-027] – After IP address is assigned, the SECC shall start the SECC Discovery Protocol server.

[V2G2-030] – After the SDP server is started successfully, SECC wait for a TLS or TCP connection.

[V2G2-033] – After TLS or TCP connection is established, SECC wait for the initialization of the V2G Communication Session.

[V2G2-034] – SECC terminate the TLS or TCP connection after stopping the V2G Communication Session.

[V2G2-724,725,727] – If the SECC received the session stop request, it terminate the data link, pause request, it pause the data link. If there are any error, it indicate an Data Link error and continue from the start point.

[V2G2-029,723,032] – When a certain time has passed, EVCC shall stop this all mechanism.

[V2G2-726] – If there are no link, whenever the SECC receives the message about Data link ready, SECC start this mechanism.

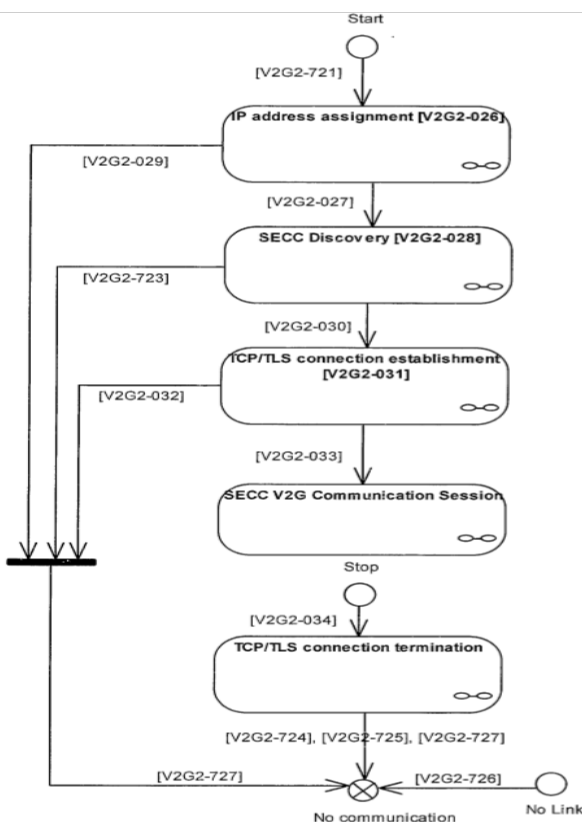


Fig. 3 Overview V2G Communication Session Status SECC

2.2.3 COMMON MESSAGE

In any charging mode defined in ISO 15118, messages defined as common messages can be applied to the message sequence. The message sequence are defined as follows.

1. Session Setup Req/Res

By using the Session Setup Request message, the EVCC establishes a V2G Communication Session. With the Session Setup Response, the SECC notifies the EVCC with

an enclosed Response Code, whether establishing a new session or joining a previous Communication Session was successful or not.

2. Service Discovery Req/Res

The Service Discovery enables the EVCC to find all services provided by the SECC. By sending the Service Discovery Request message, the EVCC triggers the SECC to send information about all services offered by the SECC. Furthermore, the EVCC can limit for particular services by using the service scope and service type elements. In case of a successful service discovery, the response lists all available services of the SECC for the defined criteria. In case the service discovery failed the service list is empty and the ResponseCode indicates potential reasons.

3. Service Detail Req/Res

By sending the Service Detail Request message, the EVCC requests, the EVCC requests the SECC to send specific additional information about services offered by the EVSE. After receiving the Service Detail Request message of an EVCC, the SECC sends the Service Detail Response message and provides details about services.

4. Payment Service Selection Req/Res

Based on the provided services and the corresponding payment options by the SECC, this message pair allows the transmission of the selected PaymentOption, SelectedServices and related ParameterSets. This request message transports the information on the selected services and on how all the selected services are paid. With the message the SECC informs the EVCC whether the selected services and payment option were accepted.

5. Payment Detail Req/Res

The payment detail message pattern is only used when some particular payment detail have to be exchanged. With the Payment Detail Request, the EVCC provides the payment details in case the selected payment was “Contract”. With the request message, the SECC informs the SECC whether the previously provided payment details were accepted or not.

6. Authorization Req/Res

If a generated challenge was sent by the SECC in a previous message, the EVCC sends back this challenge and the respective signature. Finally, the SECC verifies the challenge signature and sends the corresponding authorization response message.

7. Charge Parameter Discovery Req/Res

After being authorized for charging at the EVSE(SECC), the EVCC and the SECC negotiate the charging parameters with the ChargeParameterDiscovery Req/Res pair. By sending the request message, the EVCC provides its charging parameters to the SECC. This message provides status information about the EV and additional charging parameters, like estimated energy amounts for recharging the vehicle, capabilities of the EV charging

system and the point in time the vehicle operator intends to leave the EVSE. By response message, the SECC provides applicable charge parameters from the grid's perspective. Next to general charge parameters of the EVSE, this optionally includes further information on cost over time, cost over demand, cost over consumption or a combination of these.

8. Power Delivery Req/Res

The Power Delivery message exchange marks the point in time when the EVSE provides voltage to its output power outlet and the EV can start to recharge its battery. By sending the request message, the EVCC requests the SECC to provide power on and transmits the ChargingProfile the EVCC will follow during the charging process. After receiving the request message of the EVCC, the SECC sends the PowerDeliveryRes message including information if power will be available.

9. Certificate Update Req/Res

Updating the certificate of the EVCC is required when the certificate is still valid but is about to expire. By sending request message, the vehicle requests the SECC to deliver new certificate that belongs to the currently valid contract of the vehicle. As the response message, the SECC retrieves the requested certificate from the SA.

10. Certificate Installation Req/Res

Installing the contract certificate into the EVCC is required if EVCC currently does not possess a valid contract certificate; e.g. because no contract certificate is stored, or existing contract certificates are expired or revoked. By sending the request message, the vehicle requests the SECC to deliver the certificate that belong to the currently valid contract of the vehicles. By response message, the EVCC installs this certificate.

11. Session Stop Req/Res

This V2G message pair shall be used for terminating a V2G Communication Session initiated by preceding SessionSetupReq message. By sending the request message, the EVCC requests termination of the charging process. After receiving the requests, the SECC sends the SessionStopRes informing the EVCC if terminating the charging process was successful.

12. Metering Receipt

By sending the request message, the EVCC confirms that the data elements MeterInfo record, Session ID and the SA Schedule TupleID have been received from the SECC. After receiving the MeteringReceiptReq from the EVCC, the SECC sends the MeteringReceiptRes informing the EVCC whether the receipt was successfully received and accepted by the SECC.

2.3 ISO 15118-3

2.3.1 WHAT ISO 15118-3 DO?

- Define of V2G standardized service primitive interface.
- Cover both AC and DC use-cases.
- Describe the general requirements to the communication.
- Address how power line communication is used to modulate the digital information specified in ISO 15118-2.
- Describes a mechanism called SLAC.

2.3.2 CONNECTION COORDINATION

This clause describes the system behaviour between a plug-in and a plug-out.

A: Plug-in phase

This phase covers the plug-in up to the beginning of the charge. In EVSE side, after successful detection of the plug-in of a cable assembly, the low-layer communication module is ready for communication. In EV side, when detecting a nominal duty cycle, the EV can either start charging in the basic charging mode or wait until the HLC is established.

B: Initialization phase

When the V2G Data link setup success and the Plug and Charge identification mode is implemented, further identification is managed. According to that ID recognition, the EVSE decide whether to authorize the charge or to not authorize the charge.

C: Loss of communication

This clause covers the situation where the communication link is lost. A loss of communication after the establishment of a data link is handled by higher layers, by requesting. If the EV detects a loss of communication, it can either switch to basic charging mode or stop the charge. While relaunching the matching process, the EV may go on charging in the basic charging mode, if the EVSE sets a nominal duty cycle.

D: Sleep mode and wake-up

A sleep mode is used for energy saving. EV and EVSE can either a sleep mode after negotiating a pause through HLC protocol. On EVSE side, a sleep mode means that the oscillator will be off, the +12 V supply of the pilot line will stay on, and the low-layer communication module may be power off. On the EV side, the wake-up mechanisms may also be used after charge session was terminated. And the low-layer communication module may be powered off.

E: Plug-out phase

With the type 1 connector – the system might relaunch the communication automatically at any time. With type 2 connector – the system might relaunch the communication automatically and will relock the connector.

2.3.3 MATCHING EV – EVSE PROCESS

A unique matching between the EV and a specific charge coupler of the EVSE is necessary for most of the use cases. After this matching process success, upper layers are defined.

A: Initialization of matching process

The first phase of the matching process is called initialization of matching process. During this phase, the node is configured in order to enhance the matching process.

B: Discovery of the connected low-layer communication module

During the discovery process, the EV determines which EVSE is directly connected to its cable assembly. The method is based on a measurement of the signal strength. Only EV communication nodes shall send requests based on this signal strength method. Only EVSE communication nodes shall answer to the requests. The signal strength measurement shall be concluded by the following:

--EVSE FOUND – signal strength measurement confirm the physical matching

--EVSE POTENTIALLY FOUND – signal strength measurement does not give a distinct physical matching, validation might be required

--EVSE NOT FOUND – signal strength measurement confirms that no physical matching exists

C: Validation of matching decision

This is a method to validate the signal strength measurement. After the signal strength measurement, the EV can decide on the basis of the results to request the EVSE for an additional validation process. According to the EVSE architecture, the EVSE can answer to the request by the following certain status.

--“Not Required” state – The EV decides either to follow the EVSE recommendation and to skip the validation process or to continue the process and to perform the validation process.

--“Failure” state – The EV decides to either terminate the matching process and go on with the next EVSE or to skip the validation process with the current EVSE.

--“Ready” state – Ready to continue the validation process.

D: Set-up a logical network

According to the low-layer communication technology, a logical network might have to be built in order to enhance the communication.

E: Leave the logical network

With receiving data link terminate request from HLC, the communication shall leave the logical network. When the low-layer communication module leaves the logical network, it shall inform HLE.

F: Error handling

If some errors were found, the communication node shall leave the logical network. All parameters related to the current link shall be set to the default value and shall change to the status “Unmatched”

3. CONCLUSION

There are various problems; e.g. security and popularity, for achieving full practical use. But to realize the perfectly system of interface will solve the environment problems, and energy consumption problems. In the sense that both DC and AC charging are possible, providing SOC, ISO is expected to play a role in promoting EV in the future.

ACKNOWLEDGEMENTS

I would like to thank Professor Rajit Gadh for giving me such a valuable opportunity to study at University of California, Los Angeles. I would like to thank Doctor Peter Chu for giving me a lot of advice. To start study about Electric Vehicle, he showed me the direction of research. Moreover, I would like to thank Shashank. He gave me some papers and presentation to learn basic knowledges about Electric Vehicle.

REFERENCES

- [1] Yingqi Xiong, Road vehicles – Vehicle to grid communication interface – Part 1; General information and use-case definition(2013)
- [2] Yingqi Xiong, Road vehicles – Vehicle to grid communication interface – Part 2; Network and application protocol requirements(2014)
- [3] Yingqi Xiong, Road vehicles – Vehicle to grid communication interface – Part 3; Physical and data link layer requirements(2015)

DEVELOPMENT OF LOW ADHESION FILM USING MESOPOROUS SILICA

Takumi KANI

Department of Micro-Nano Mechanical Science and Engineering, Graduate School of Engineering, Nagoya University

kani@ume.mech.nagoya-u.ac.jp

Supervisor: Laurent Pilon

Department of Mechanical and Aerospace Engineering, University of California, Los Angeles

pilon@seas.ucla.edu

ABSTRACT

Slippery liquid-infused porous surface (SLIPS) are nature inspired surfaces. These surfaces were developed with the aim of exceptional liquid- and ice-repellency and pressure stability. Typically, these surfaces are composed of a combination of porous film and lubricant oil. In this research, we tried to develop new SLIPS using mesoporous silica film and PFC liquid. Mesoporous silica films are prepared with sol-gel method. Subsequent infusion of perfluorocarbon lubricants (Krytox106) into the porous structure results in liquid-repellent slippery surfaces. To test the ability of the coating to repel water, water contact angle and sliding angle measurements were conducted.

1. INTRODUCTION

Currently there are a lot of development of synthetic liquid-repellent surfaces inspired by the lotus effect [1]. The principle of the lotus effect is to create textured surfaces that enable water droplets to easily roll off of the surface. These developments improve both surface water repulsion and hydrophobicity. However, while this approach is promising, it suffers from limitations that severely restrict its applicability. First, the air trapped within the texture cannot stand up to pressure. As a result, the liquid can easily soak into the texture under even slightly increased pressures [2]. Second, synthetic textures are easy to cause serious defects arising from mechanical damage and fabrication imperfections [3]. To solve these problems, slippery liquid-infused porous surface (SLIPS) are developed under the influence of Nepenthes pitcher plant [4]. In pitcher plants, this film is aqueous and effective enough to cause insects that step on it to slide from the side wall into the digestive juices at the bottom by repelling the oils on their feet. Inspired by this idea, Wong, T.-S., *et. al* reported SLIPS that each consist of a film of lubricating liquid locked in place by a micro/nano porous substrate. The characteristics of this

surface coating are ease of peeling of liquid and ice, pressure stability, self-healing, and optical transparency because of filling the surface structure with oil. These surface coatings are assumed to be useful in various fields. For example, these surfaces will be useful in fluid transportation, medicine, inside the food container and as self-cleaning and antifouling materials operating in extreme environments.

In this study, mesoporous silica was used as the porous surface, and PFC (perfluorocarbon) liquid (Krytox106), was used as the lubricating oil. Mesoporous silica has been widely studied due to its simple synthesis and easily controlled structural properties. PFC liquid is a hydrocarbon with all hydrogen atoms replaced with fluorine atoms. These oils create high density, omniphobic interfaces. By using these materials, we suggest to create SLIPS by a simple method at low cost [5].

2. EXPERIMENTAL PROCEDURE

2.1 MODEL OF SLIPS

SLIPS creates an omniphobic surface by preventing outside liquids from penetrating the surface structure to the Wenzel state. The Wenzel state is a state in which droplets penetrate surface structures and provide high adhesion. When the porous structure is filled with lubricant instead of air, the slippery liquid in the porous solid helps the surface structure become Cassie-Baxter state. The Cassie-Baxter state is a state in which droplets cannot penetrate surface structures. Instead, water droplets remain on rough structures, trapping air beneath them. [6] The difference between Wenzel and Cassie-Baxter states is illustrated in Figure 1. This phenomenon is also exploited in many superhydrophobic surfaces where an air cushion is entrapped within the porous solid surface. As a result of, spherical water drops easily roll off the surface [7].

When we consider the case where a composite surface is made of A with contact angle θ_a and B with contact angle θ_b .

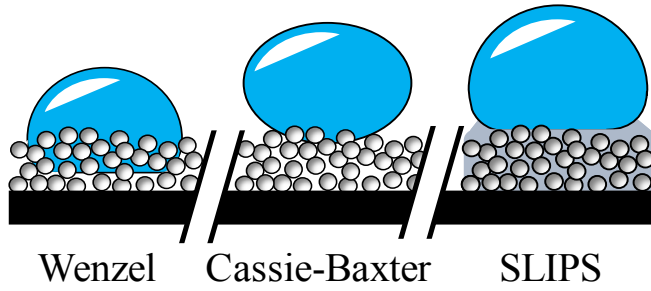


Figure 1 The difference between Wenzel, Cassie-Baxter state and SLIPS

In this case, the surface area of A and B described f_a : f_b . f_a and f_b represent the specific surface area of A and B, respectively ($f_a + f_b = 1$). It is described that the surface tension between solid and gas γ_{SG} , and the interfacial tension between solid and liquid γ_{SL} , each is written as follows.

$$\gamma_{SG} = f_a \cdot \gamma_{SG,a} + f_b \cdot \gamma_{SG,b} \quad (1)$$

$$\gamma_{SL} = f_a \cdot \gamma_{SL,a} + f_b \cdot \gamma_{SL,b} \quad (2)$$

And the Young's formula for contact angle and surface tension is described as follows.

$$\gamma_{LG} \cos \theta + \gamma_{SL} = \gamma_{SG} \quad (3)$$

So, the contact angle of the composite surface (φ) can be shown equation 4

$$\cos \varphi = f_a \cdot \cos \theta_a + f_b \cdot \cos \theta_b \quad (4)$$

If B is air, $\theta_b = 180^\circ$, $f_b = 1 - f_a$ so the contact angle (φ_{air}) can be shown equation 5.

$$\cos \varphi_{air} = f_a \cdot \cos \theta_a + f_a - 1 \quad (5)$$

2.2 SYNTHESIS OF SLIPS

Synthesis of mesoporous silica films. The following materials were obtained from commercial suppliers and used without further purification: colloidal suspension of SiO₂ nanoparticles (15 wt %, Nalco2326, ammonia-stabilized colloidal silica, $d=5$ nm, NalcoChemical Company), triblock copolymer Pluronic P123 (EO₂₀PO₇₀EO₂₀, $M_w=5800$ Da, BASF), triblock copolymer Pluronic F127 (EO₁₀₀PO₆₅EO₁₀₀, $M_w=12600$ Da, BASF), tetraethyl orthosilicate (98%, Acros Organics), hydrochloric acid (Certified ACS Plus, Fisher Scientific), and ethanol (200 proof, Rossville Gold Shield).

Sol-gel based mesoporous silica thin films were prepared by polymer templated evaporation-induced self-assembly in Figure 2 as reported previously in literature [5],[8]. Tetraethyl orthosilicate (TEOS) was used as a silica precursor while the triblock copolymer Pluronic F127 were used as the structure-directing agents. First, 50.1 mg of Pluronic F127 was dissolved in 0.6 mL of ethanol and 0.16 mL of 0.1 M HCl. 0.122 ml of tetraethyl orthosilicate (TEOS) was added to the mixture. Then, 80 μ L of the polymer-silica solution was spin-coated onto a 1×1 in²

glass substrates. Upon evaporation, the system self-assembled into an organic-inorganic nanocomposite. The film thickness was adjusted by controlling the spin speed. To make uniform thin mesoporous silica films, spin-coating was performed at 1000 rpm for 50 seconds and 3000 rpm for 20 seconds. Subsequently, the nanocomposite films were calcined to remove the block copolymer and develop the mesoporous structure. The films were then heated at 180 °C for 6 hours to dry and age the film then the dried films were calcined in air at 350 °C for 30 min to remove the polymer.

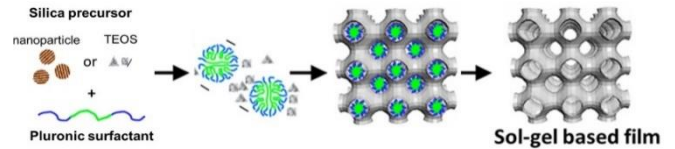


Figure 2 Synthesis of Sol-Gel Based Mesoporous Silica Films Produced via Evaporation Induced Self-Assembly

Liquid-infused slippery surfaces. The PFC liquid used as the liquid substrates were perfluoropolyether liquids Krytox GPL 106 (Miller-Stephenson Chemical Company Inc., Danbury, CT) with general formula $[\text{CF}(\text{CF}_3)\text{CF}_2\text{O}]_n$ where $n = 10-60$ [9]. The mesoporous silica surface was coated with a thin layer of PFC using perfluorosilane to allow the PFC liquid to penetrate more into the pores. The PFC layer interact with the PFC liquid better since they are similar in structure. Samples were briefly exposed (40 s) to oxygen plasma in order to gently activate the surface to react with the perfluorosilane. Immediately following plasma activation, samples were immersed in a liquid silane solution (5% v/v tridecafluoro-1,1,2,2-tetrahydrooctyl trichlorosilane) in ethanol for 1 h at room temperature. Treated samples were rinsed with ethanol, deionized water, and three times with pure ethanol. Rinsed samples were gently blown dry with compressed nitrogen and gently heated in an oven with desiccant at 60 °C overnight at atmospheric pressure [10]. Then an excess amount of a PFC liquid was applied onto the mesoporous silica surface. The liquid was maintained on the surface for less than 6 hours to fully saturate the pores in the polymer. Afterward, samples were spin-coated at 1000 rpm for 50 seconds and 3000 rpm for 20 seconds to get rid of the excess of PFC liquid lubricant before use in the experiments for measuring the water contact angle.

2.3 DEVICE OF SLIDING ANGLE MEASUREMENT

Schematic view of device we designed and machined to measure sliding angle is shown in Figure 3. An aluminum stage was designed to be able to measure the sliding angle easily by attaching it to a tilt stage, and was made to measure one sample with one measurement. By twisting the knob of the tilt stage, the sample and stage are rotated and can measure the sliding angle. The produced device is shown in Figure 4.

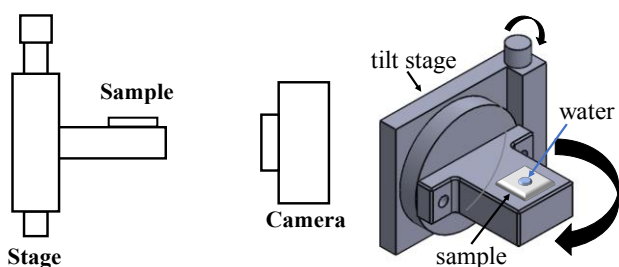


Figure 3 Schematic view of device to measure sliding angle

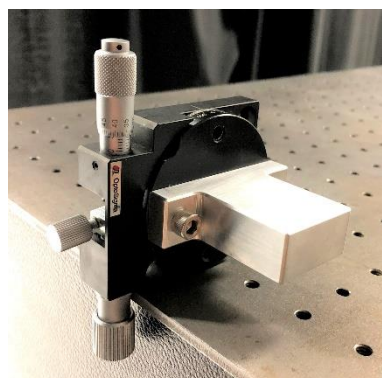


Figure 4 Device to measure sliding angle

3. RESULT AND DISCUSSION

3.1 SEM IMAGE OF POROUS FILM

Scanning Electron Microscopy (SEM) images were obtained using a model JEOL JSM-6700F field emission electron microscope with 5 kV accelerating voltage and secondary electron detector configuration. The pictures of mesoporous silica film are shown in Figure 5. From Figure 5 (a), it was shown that the mesoporous silica film with random porous material was made by the sol-gel based method in 2.2. Figure 5 (b) shows that the whole film is made of porous material by observing not only the surface but also the side view by making a scratch on film at the time of observation.

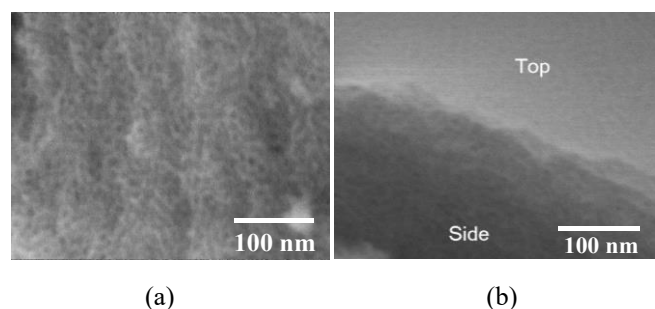


Figure 5 (a) Mesoporous silica film (b) Scratch with film

3.2 CONTACT ANGLE

The surfaces were tested with a contact angle meter (KSV Instruments CAM 200) to characterize the water contact angle θ_c . The water contact angle testing was carried out with 5 μ l water droplet. Measurements were performed for four different surfaces: glass, glass with mesoporous silica film, PFC liquid with plain glass, and the complete SLIPS, which has both mesoporous silica film and PFC liquid. The measurements were performed at two different points for each sample. The θ_c measurements show that the apparent contact angles between the water droplet and both PFC oiled surfaces are similar. PFC liquid forms an annular wetting uplift around the water droplet, preventing us from seeing the real contact angles. Therefore, spin-coating was performed after infusing the PFC liquid to remove an excess PFC liquid. As a result, an excess PFC liquid was removed as much as possible, and we succeeded in reducing the wetting uplift around the water droplets caused by PFC liquid. Then we were able to observe contact angle close to the actual contact angle. Figure 6 shows the contact angle with and without spin-coat after infusing PFC liquid. Figure 7 shows the water contact angle of four samples with spin-coat after infusing PFC liquid.

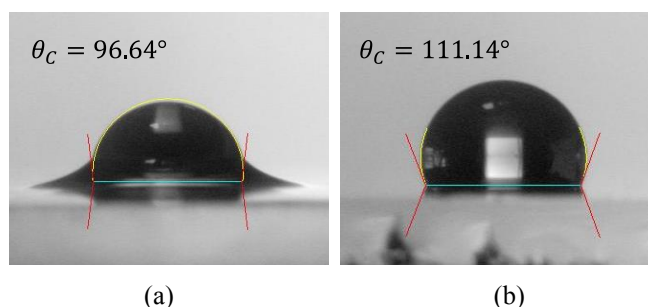


Figure 6 (a) Without spin-coated after infusing PFC liquid, (b) With spin-coated after infusing PFC liquid

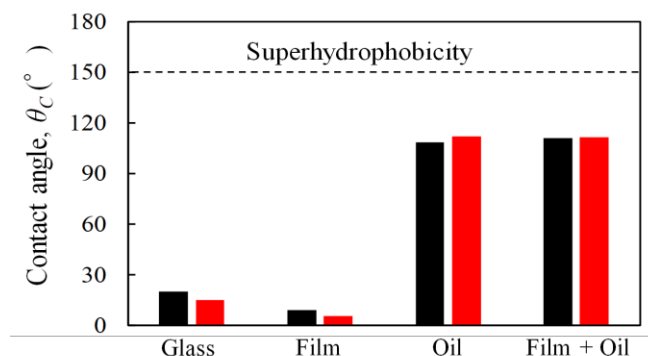


Figure 7 Water contact angle measurements

3.3 SLIDING ANGLE

3.3.1 RESULTS OF SLIDING ANGLE

The surfaces were tested with a device we made to characterize the water sliding angles θ_s . The water sliding angle measurements were carried out using water droplets of different volumes. The sliding angle measurements, like the contact angle measurements, were performed on four different surfaces. The samples were fixed with double-sided tape. The sliding angles were measured in the range from 0° to 90° , and, if no sliding was observed, the droplet was deemed pinned to the surface. The volume of water droplet used with glass and glass with mesoporous silica film ranged from $10\ \mu\text{l}$ to $80\ \mu\text{l}$ while for the samples made with PFC liquid on plain glass, and the complete SLIPS (which has both mesoporous silica film and PFC liquid), $10\ \mu\text{l}$ to $20\ \mu\text{l}$ of water was used. The sliding angle measurements were carried out without removing excess PFC on the surface. Figure 8 shows the water sliding angle of each sample.

From Fig. 8, it can be said that the presence of PFC liquid as a lubricant on the surface greatly affects the sliding angle. From the comparison of the four samples in Figure 8, water droplet slid on the SLIPS coating at a small angle even with the smallest amount of water droplets. Figure 8 (a) and (b) show that there is a relationship between the amount of water droplet and the sliding angle. This is considered to be because the amount of water is an important factor in the sliding angle measurement, and the interfacial tension between the sample surface and the water droplet is larger than the gravity acting for the water droplet to slide down with a small amount of water droplet [11].

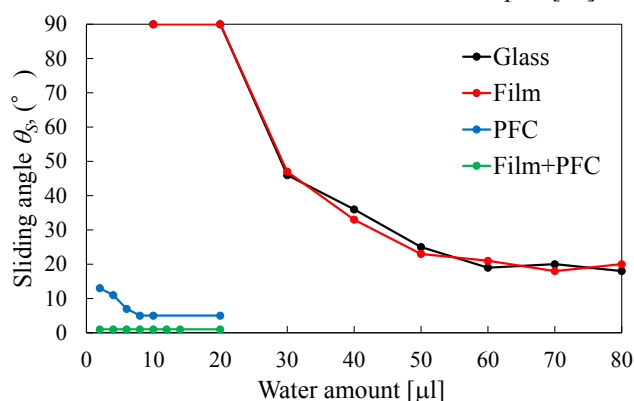


Figure 8 Water sliding angle measurements

3.3.2 DIFFERENCE BETWEEN SLIPS AND GLASS+PFC

With PFC liquid on plain glass, after the sliding angle was measured, the high contact angle of the water droplet was not maintained as observed by the water spreading. Therefore, PFC liquid needed to be reapplied after each measurement. This is considered that because the PFC on the glass became non-uniform and the glass was appeared on the surface by repeating the experiment. However, in

SLIPS, a high contact angle was stably maintained even after a water droplet was collected from the same sample and then dropped again. Figure 9 shows the comparison image of PFC liquid with plain glass and SLIPS. This leads to a reduction in the number of times of adding PFC liquid as a lubricant. It is thought that the reasons for the stable high contact angle obtained with SLIPS is the self-healing property. The mesoporous silica surface was coated with a thin layer of PFC using perfluorosilane to allow the PFC liquid to penetrate more into the pores. The PFC layer interact with the PFC liquid better since they are similar in structure. For this reason, the reactivity with PFC was higher than that of glass, and it is considered to be possible to quickly repair the damaged part of PFC when the measurement was repeated. And the lubricating film also serves as a self-healing coating to rapidly restore the liquid-repellent function following damage of the porous material. The fluidic nature of the lubricating layer means that the liquid simply flows towards the damaged area by surface-energy-driven capillary action, and spontaneously refills the physical voids [4]. It is considered that the PFC liquid flowed into the damaged area when collecting water droplets, and maintained a uniform surface with PFC liquid.

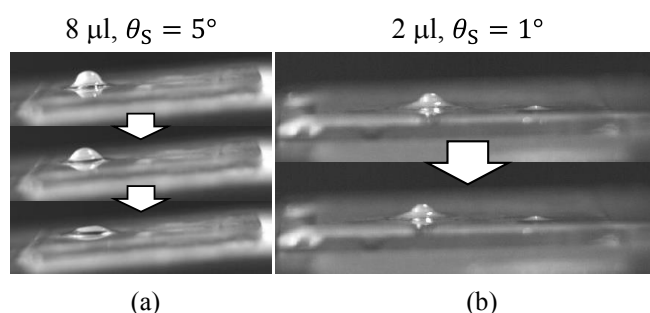


Figure 9 (a) PFC liquid with plain glass, (b) SLIPS

3.4 DIFFERENCE OF FILM THICKNESS

As explained in Section 2.2, the thickness of mesoporous silica film can be adjusted by controlling the spin speed. We prepared three samples that were spin-coated at 1000 rpm for 50 seconds, then 3000 rpm for 20 seconds, 1000 rpm for 50 seconds then 6000 rpm for 20 seconds and 1000 rpm for 50 seconds then 8000 rpm for 20 seconds. The thickness of the films was measured using a surface profiler (Dektak 150 Veeco, Plainview, USA). The thickness of films was measured at three points of each sample, and the average value was used. Table 1 shows the relationship between spin speed and thickness of film. Then, the contact angle and the sliding angle were measured in the same way as in 3.3 and in 3.4 using the samples with these three thicknesses of films. Figure 10 shows the results of the contact angle at different thickness of mesoporous silica film. Figure 11 shows the results of the sliding angles at different thickness of film. From Figure 10 and 11, there was no difference in the results of the contact angle and the sliding angle regarding the difference of the mesoporous silica film thickness.

Table 1 Film thickness of mesoporous silica

Spin speed (rpm)	Thickness of film (nm)
3000	650
6000	417
8000	333

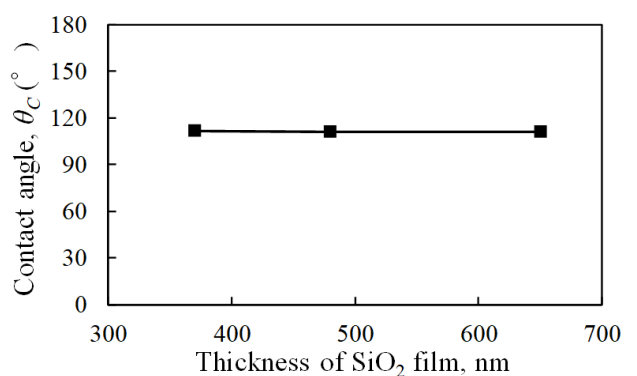


Figure 10 Water contact angle at different film thicknesses

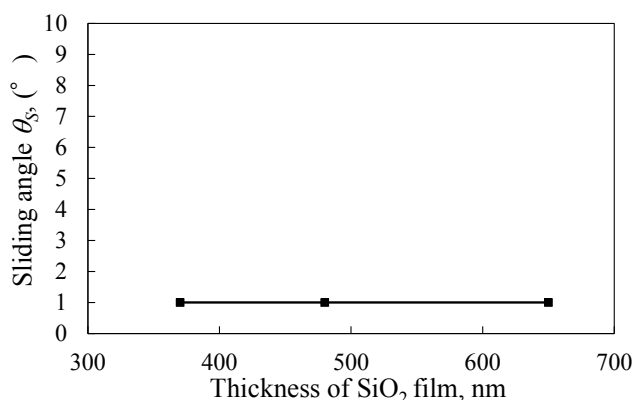


Figure 11 Water sliding angle at different film thicknesses

4. CONCLUSION

We tried to develop a surface coating with low adhesion using mesoporous silica film and PFC liquid based on a model called SLIPS inspired by nature. As a result of measuring the contact angle and the sliding angle of four samples, the sample made based on SLIPS was the most stable and slippery. And there was no difference in the contact angle and the sliding angle depending on the thickness of mesoporous silica film. In future work, however the angle was evaluated in this research, it is considered necessary to evaluate the sliding speed of the water droplet. In addition, as a future work, it is necessary to clarify the relationship between porosity, pore size and hydrophobicity.

ACKNOWLEDGEMENTS

I would like to thank Professor Laurent Pilon for giving me a great opportunity to study in University of California,

Los Angeles. I would like to thank Sophia King, Tiphaine Galy, Eylul Simsek, and Bradley Stewart for supporting this research. I really appreciate their guidance and kindness. Also, I would like to thank all of lab members for their kindness. I would like to thank staffs in the department of Mechanical and Aerospace Engineering for supporting my work. This work was supported by Japan-US-Canada Advanced Collaborative Education Program. Finally, I appreciate my supervisor, Prof. Noritsugu Umehara, for allowing me to join this program.

REFERENCES

- [1] W. Barthlott, and C. Neinhuis. "Purity of the sacred lotus, or escape from contamination in biological surfaces." *Planta* 202.1 (1997): 1-8.
- [2] N. Nguyen, T. Phuong, *et al.* "Quantitative testing of robustness on superomniphobic surfaces by drop impact." *Langmuir* 26.23 (2010): 18369-18373.
- [3] L. Bocquet, and E. Lauga. "A smooth future?" *Nature materials* 10.5 (2011): 334.
- [4] T. S. Wong, *et al.* "Bioinspired self-repairing slippery surfaces with pressure-stable omniphobicity." *Nature* 477.7365 (2011): 443.
- [5] Yan, *et al.* "Exploring the Effect of Porous Structure on Thermal Conductivity in Templated Mesoporous Silica Films." *The Journal of Physical Chemistry C* 123.35 (2019): 21721-21730.
- [6] A. B. D. Cassie, and S. Baxter. "Wettability of porous surfaces." *Transactions of the Faraday society* 40 (1944): 546-551.
- [7] X. M. Li, D. Reinhoudt, and M. Crego-Calama. "What do we need for a superhydrophobic surface? A review on the recent progress in the preparation of superhydrophobic surfaces." *Chemical Society Reviews* 36.8 (2007): 1350-1368.
- [8] Dunphy, Darren R., *et al.* "Enlarged pore size in mesoporous silica films templated by pluronic F127: Use of poloxamer mixtures and increased template/SiO₂ ratios in materials synthesized by evaporation-induced self-assembly." *Chemistry of Materials* 27.1 (2014): 75-84.
- [9] M. Marszewski, *et al.* "Thick Transparent Nanoparticle-Based Mesoporous Silica Monolithic Slabs for Thermally Insulating Window Materials." *ACS Applied Nano Materials* 2.7 (2019): 4547-4555.
- [10] Leslie, C. Daniel, *et al.* "A bioinspired omniphobic surface coating on medical devices prevents thrombosis and biofouling." *Nature biotechnology* 32.11 (2014): 1134.
- [11] E. Wolfram and R. Faust, in "Wetting, Spreading, and Adhesion," ed. by J. F. Padday, Academic Press, London (1978), Chap. 10.

Conditional Machine Learning-Based Inverse Design of Photonic Metasurfaces

Yusaku Kawagoe

Department of Mechanical System Engineering, Graduate School of Engineering, Nagoya University
kawagoe.yusaku@g.mbox.nagoya-u.ac.jp

Project team members and Supervisor: Christopher Yeung, Ju-Ming Tsai, and Aaswath Raman

Department of Materials Science and Engineering, University of California
cyyeung1234@ucla.edu, aaswath@ucla.edu

ABSTRACT

Reaching the true potential of nanophotonic structures for exciting applications such as invisibility cloaking, perfect lenses, and light trapping for solar cells requires the design of intricate devices that can precisely control the behavior of incident light. However, existing "forward design" methods rely on human intuition and numerous trial-and-error optimization. In contrast, "inverse design" methods show great potential in producing direct solutions, but are computationally expensive and are more likely to miss locally optimal designs [1]. To overcome the limitations of current inverse design paradigms, we present a conditional deep convolutional generative adversarial network (DCGAN) that produces nanophotonic structures through inverse design. Compared to conventional simulation-based methods, the presented machine learning-based method can achieve a wider array of designs, which meet a target spectrum, in a fraction of the time and with far fewer computational resources.

Undisclosed

STUDY ON TRIBOLOGICAL PERFORMANCE OF ALUMINUM ALLOY 7075(T6)-TiB₂ NANOCOMPOSITES

Tomohiro Saso

Department of Micro-Nano Mechanical Science and Engineering, Graduate school of Engineering, Nagoya University
sasot@ume.mech.nagoya-u.ac.jp

Supervisor: Prof. Xiaochun Li

Department of Mechanical and Aerospace Engineering, University of California-Los Angeles
xcli@seas.ucla.edu

ABSTRACT

In this work, the tribological performance of AA7075(T6) and AA7075(T6)-1.5 vol.% TiB₂ nanocomposites was studied. The dry friction test was done using a newly developed high-resolution friction force collecting system enabled by a high-resolution laser displacement system under a fixed load of 0.27 N with 4 different friction counterparts (AA5083, Fe-A247, Fe-52100, and Si (wafer)), and the true and reliable tribological performance of AA7075-TiB₂ nanocomposites has been evaluated. All of the samples and counterparts were polished to sub-micron surface roughness, in order to rule out the effect of roughness on the coefficient of friction (CoF). The result of the friction tests has shown that both the increase and decrease of CoF with different counterpart hardness for AA7075(T6) and AA7075(T6)-1.5 vol.% TiB₂ exist, and no simple trend is observed when the counterpart hardness is changed. Significantly, with Si as a counterpart, AA7075(T6)-1.5 vol.% TiB₂ nanocomposite has shown a ~22 % lower CoF value than AA7075(T6). We concluded the CoF change is greatly affected by the hardness combination of the sample and the counterpart. This understanding will be important for the applications of metal matrix nanocomposites in tribo-related fields.

Undisclosed

TOWARD ROBUST TUNING OF INTEGRAL RESONANT CONTROL

Takeshi Matsumoto

Department of Mechanical Systems Engineering, Graduate School of Engineering, Nagoya University
matsumoto.takeshi@f.mbox.nagoya-u.ac.jp

Supervisor: Tetsuya Iwasaki

Department of Mechanical and Aerospace Engineering, University of California, Los Angeles
tiwasaki@ucla.edu

ABSTRACT

This paper considers a design method for the integral resonant control, which is a relatively new and effective vibration control method for lightly-damped flexible structures. The proposed design method only requires frequency response data of the flexible structure. Validation of the proposed design procedure is demonstrated with an experiment using a lightly-damped plate structure and piezoelectric elements.

Undisclosed

Effects of Pulse Width of VNbTaMoW High Entropy Alloy Thin Films Deposited by HiPIMS

Tomoyasu WATANABE

Department of Micro-Nano Mechanical Science and Engineering, Graduate School of Engineering, Nagoya University
watanabe@ume.mech.nagoya-u.ac.jp

Supervisor: Suneel Kodambaka

Department of Materials Science and Engineering, University of California, Los Angeles
Kodambaka@ucla.edu

ABSTRACT

In this research, we deposited VNbTaMoW high entropy alloy (HEA) thin films by using direct current magnetron sputtering (DCMS) and high power impulse magnetron sputtering (HiPIMS) to study especially the influence of pulse width in the latter sputtering on structure of the films. For pulse width ranging from 25 μ sec to 400 μ sec, the deposition rate, morphology and crystal structure were analyzed. All films showed the formation of a solid solution with body-centered cubic structure regardless of deposition method and pulse width. We found that the deposition rate by using HiPIMS was lower than by using DCMS, and there was not much difference in deposition rate due to pulse width. We also observed that HEAs 222 peaks appeared by changing pulse width even under same temperature and average power condition. Our results demonstrate microstructural and crystallinity tunability during sputter-deposition of HEA thin films changing pulse width.

Undisclosed

Finite Element Analysis of Contact in Asperities

Takaaki Miyachi

Department of Mechanical and Industrial Engineering, Graduate School of University of Toronto, Canada

takaaki@mie.utoronto.ca

Supervisors: Shaker A. Meguid¹ and Noritugu Umehara²

¹Department of Mechanical & Industrial Engineering, University of Toronto

meguid@mie.utoronto.ca

²Department of Micro-Nano Mechanical Science and Engineering, Nagoya University

ABSTRACT

Friction in sliding and rotating parts of machines such as automobiles is the principle cause of energy dissipation and low efficiency. Wear and material transfer at the contact surfaces due to friction can lead to fretting failures. Fretting accelerate fatigue failure of components by creating crack initiation sites on the surface. It is therefore important to critically assess and determine the parameters that governs the mechanical integrity of contact surfaces. In this paper, to study the sliding interactions between contact surfaces, we carried out 2D and 3D finite element analysis to examine the sliding interaction between two surfaces. The roughness of these surfaces was idealized into periodic sinusoidal shape. It was found that as the amplitude of the asperities increase the contact area decreased. On the contrary, as the wavelength increase, the contact area increase. Conclusively, rough surfaces increase the extent of permanent deformation and reduce the contact surface area.

1. INTRODUCTION

The movement of one solid surface over another is fundamentally important to the operation of many kinds of mechanisms. Tribology is the study of surface interactions in systems sliding and rolling against each other. Although tribology is a much wider than the study of friction, it plays a crucial role in the performance of many mechanical systems. Low friction is desirable and essential in bearings and gear systems to increase efficiency and reduce energy loss through the dissipation of heat. However, low friction is not necessarily needed in all systems. For example, controlled friction is needed in the operation of brakes and clutches to dissipate kinetic energy and transfer torque, respectively.

The law of friction states that frictional force is proportional to the normal load. Furthermore, the frictional force is independent of the apparent area of contact and sliding velocity. The coefficient of friction is defined as:

$$\mu = F/W \quad (1)$$

where F and W is defined as the frictional force and normal force, respectively. The coefficient of friction is characteristic of tribological system but is not material characteristic [1].

Two types of friction coefficients can be distinguished: one that represents the friction opposing the onset of relative motion (impending motion), and one that represents the friction opposing the continuance of relative motion once that motion has started. The former is called the static friction coefficient, and the latter, the kinetic friction coefficient. In the case of solid-on-solid friction (with or without lubricants), these two types of friction coefficients are conventionally defined as follows:

$$\mu_s = F_s/W \quad (2)$$

$$\mu_k = F_k/W \quad (3)$$

where F_s is the force just enough to prevent the relative motion between two bodies, F_k is the force needed to maintain relative motion between two bodies [2].

The effect of friction is dependent on many factors. For example, the sliding behaviour and friction between two surfaces are influenced by the surface roughness, surface contact area and relative speed of the contact surface [3,4]. During sliding, the coefficient of friction is dependent on the surface texture and roughness parameters such as R_a . Menezes et al. [5] performed inclined pin-on-plate sliding experiments. He studied the effect of surface texture in controlling frictional behaviour. He concluded that softer material surface textures showed larger variations in friction between ground and polished surfaces. Unlu et al. [6] measured the friction coefficient of journal bearing. He showed that coefficient of friction increased with increasing velocity in dry friction and decreased with increasing normal load.

Other factors affecting friction behaviour were also investigated using finite element model (FEM). For example, Zhang et al. [7,8] examined the effect of friction and relative speed of contact surface sliding across each other on sheet metal forming. The surface roughness of contact surfaces was

represented by idealised periodic sinusoidal wave. One of the surfaces was assumed to be rigid and the other deformable. Lee [9] developed a dry friction model and showed that the coefficient of friction increased as roughness increased. Hassan and Adams [10] used an elastic-plastic 3D FEM to study the interaction of two nearby interacting asperities. However, these works are often limited to two-dimensional problems. Three-dimensional FEM only considered one asperity and did not consider the interactions of multiple asperities. Therefore, to address these deficiencies, we developed both 2D and 3D FEM model. In the 2D model, surface roughness was represented by idealised period sine wave to study the effect of amplitude and wavelength of asperity on the contact area. Since the 2D model is less computationally expensive, we were able to simulate contact of micro asperities with finer mesh. In the 3D model, the surface geometry was simplified from a typical fractal geometry using two different sinusoidal functions [11] as illustrated in Fig. 1. The equations of the functions were sketched in perpendicular planes and both smooth and rough asperities (Fig. 2) was generated according to these equations:

Smooth

$$y(x) = 0.05 \cos(40\pi x) \quad (1)$$

Rough

$$y(x) = 0.05 \cos(8\pi x) + 0.01 \cos(40\pi x) \quad (2)$$

The 3D model is a more realistic representation of surfaces in contact.

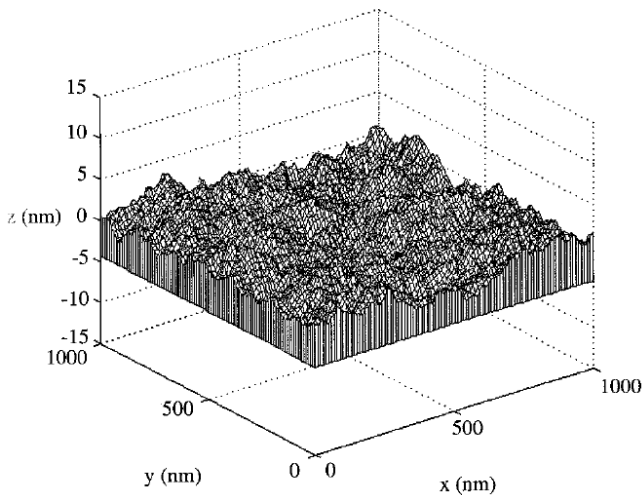


Fig. 1: Typical fractal asperity surface [11]

2. FINITE ELEMENT MODEL DETAILS

2.1 Geometry and Material Properties

The micro-mechanical behaviour of sliding between rough and deformable surface were studied using the finite element software ANSYS. The 2D and 3D geometry in this work was generated in Design Modeller and SOLIDWORKS, respectively. The calculations were carried out at the micro-meter scale. Reproducing a real interface shape in the model would considerably increase the effort required to generate a

suitable mesh and the size of the calculation domain needed to represent different rugosity shapes. Consequently, long calculation times would be required. For these reasons, the roughness in the numerical simulations were assumed to be perfect and period. Therefore, periodicity boundary condition were used of the model as shown in Fig. 2.

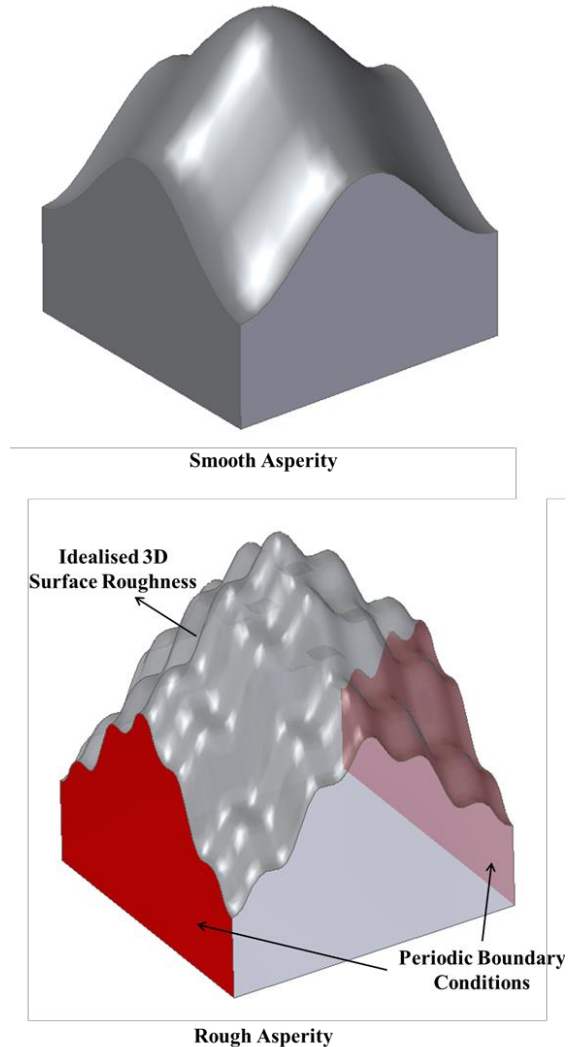


Fig. 2: Periodic Boundary conditions in 3D FEM in ANSYS workbench

In the 2D model, we varied the roughness by changing the amplitude A of the undulations from $1 \mu\text{m}$ to $2 \mu\text{m}$, and the wavelength W from $18 \mu\text{m}$ to $30 \mu\text{m}$. The idealised surface for the 3D model were described in section 1 using equation (1) and (2). A realistic material choice for this problem is elastic-plastic austenitic stainless steel which is typically used in bearing applications. The plastic behaviour of this material was obtained from a summary paper of over 600 tested samples of stainless steel [12]. The data points were manually input into a table in ANSYS engineering data section under “multilinear isotropic hardening”. Table 1 shows the material properties used in this simulation.

Table 1: Material Property of austenitic stainless steel [12]

Properties	Values
Young's Modulus (GPa)	207

Poisson's Ratio	0.3
Yield Stress (MPa)	270
Plastic Strain (mm/mm)	Stress (MPa)
0.004	300
0.01	330
0.1	460
0.3	610
0.5	660

The 2D model was meshed with Plane 183 plane strain elements in ANSYS. Plane 183 is a higher order 2-D, 8-node or 6-node element. The 3D model was meshed with Solid 186, 10-noded quadratic tetrahedral elements. A mesh convergence study was conducted and discussed in section 3.

2.2 Contact details

The most important step in pre-processing was defining the contact type. For this analysis, frictional contacts were used with Augmented Lagrange formulation. For the 3D model, the contact regions were defined as shown in Fig. 3 and their behavior was set to symmetric. To reduce the computational time, face splitting was done so that only the area that will make contact were selected. Symmetric behavior allows ANSYS to treat each contacting surface as both a contact and a target. Although symmetric behavior is more computationally expensive, it reduces the contact penetration of either surface through the other. The pinball radius was left to be defined automatically by the program. This parameter affects if a node on a target surface is in "near" contact and will monitor its relationship to the contact detection point more closely (whether contact is established). Nodes on target surfaces outside of this sphere are not monitored closely for that contact detection point. A contact tool was added, and the initial contact state was checked to ensure that no penetration or a gap which was too large existed before the simulation began. Frictional contact is applied to the bottom surface of upper body and the top surface of lower body with a constant friction coefficient.

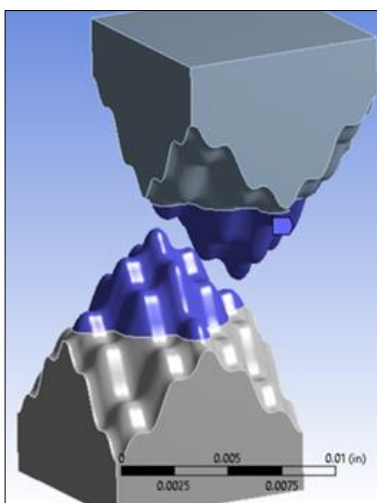


Fig. 3: Contact area selected using face splitting to reduce computation time

The small-sliding option reduces solution cost and improves solution robustness, however for this situation it is not appropriate as the expected sliding is not small. The mesh quality at the contact interfaces is assumed sufficiently refined to disable the small sliding option which would otherwise aid in convergence.

2.3 Loading and Boundary Conditions

Fixed support was added to the bottom surface of lower body in both the 2D and 3D model, to ensure that it does not move while a displacement in the x-direction was applied to the upper body causing contact. The displacement in the x-direction at each load step were modified to improve convergence and reduce computation time. To prevent the model from rotating during the displacement, the remote displacement in y and z directions was set to 0. In the 2D model, in addition to the displacement, a normal load of 1 N are applied to the top surface of upper body for sliding between the two surfaces. As illustrated in Fig. 4.

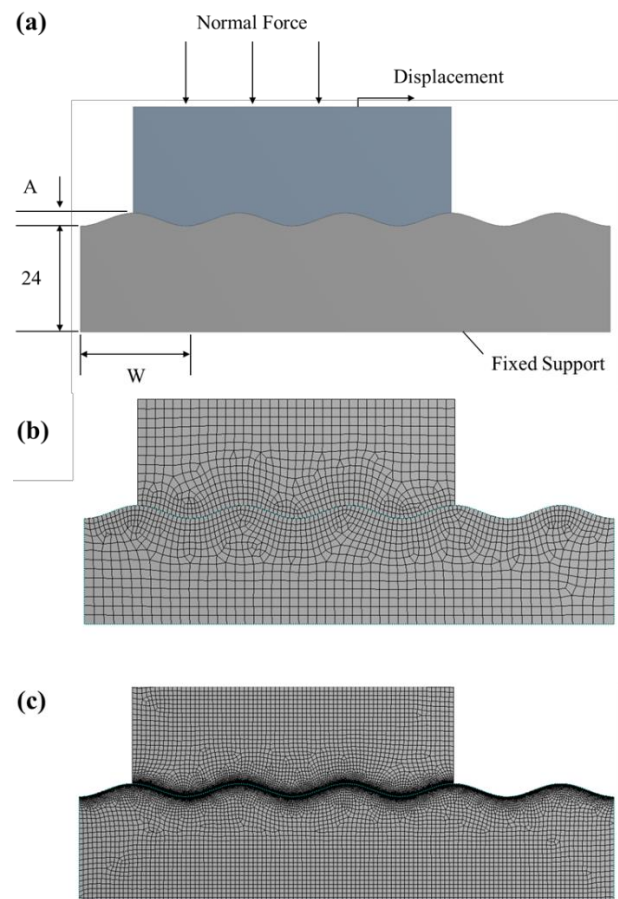


Fig. 4: 2D Finite element model (a) solid geometry, (b) coarse mesh and (c) fine mesh

Figure 5 summarised the FEM approach used in this paper.

3. Results and Discussions

3.1 Sensitivity Analysis

The element size in the 2D and 3D model is determined following convergence analysis as summarised in Table 2 and

3, respectively. To reduce computational cost, only the area where contact occurs were mesh with the selected mesh size. The selected element size is highlighted in the tables.

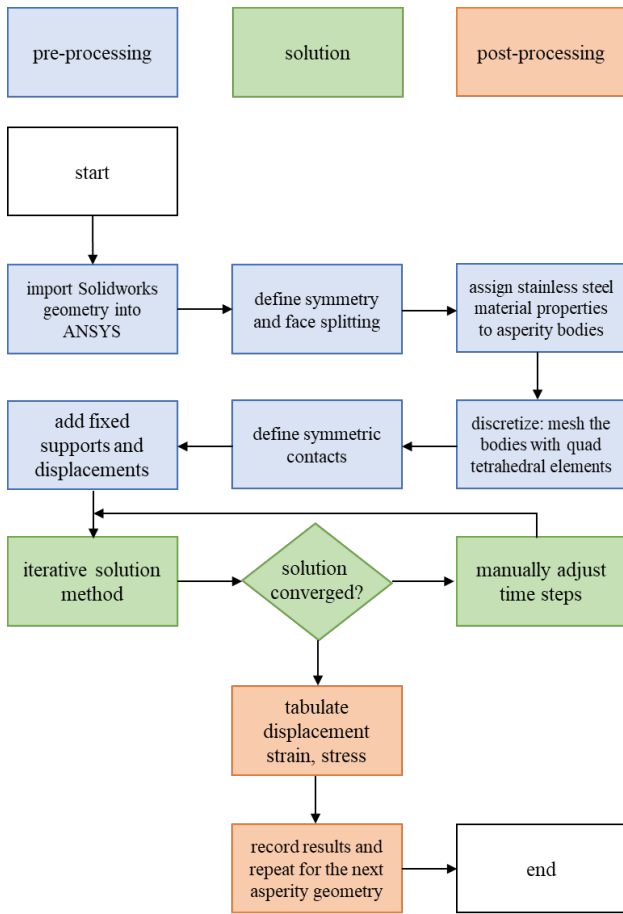


Fig. 5: Finite Element Method Approach

Table 2: Element size convergence for 2D Model

Element Size (μm)	Max Strain (mm/mm)	Contact Area (μm)
1	0.00038	11.9
0.5	0.00038	16.9
0.1	0.00038	17.3
0.05	0.00038	17.4

Table 3: Element size convergence for 3D Model

Element Size (μm)	Max Stress (MPa)
15	215
10	218
5	219

3.2 Effect of Amplitude and Wavelength on Contact Area

Figure 6 shows the distribution of von Mises stress plot for a roughness with an amplitude of 1.5 μm and wavelength of 24 μm for the 2D model. The maximum local pressure was .2 MPa, the average pressure was 9.5 MPa, and the maximum

deformation was about 0.02 μm. The results were compared to the result in [7] and the von Mises stress distribution is similar. In this paper, static friction analysis was performed using a small displacement to reduce plastic deformation, but the analysis conducted in [7] was performed at a relative speed of 20 m/s and a time of 2.25 μs. In this research, our focus is to analyse the effect of surface shape and roughness on contact stresses, therefore we only applied a small displacement to reduce the amount of surface deformation.

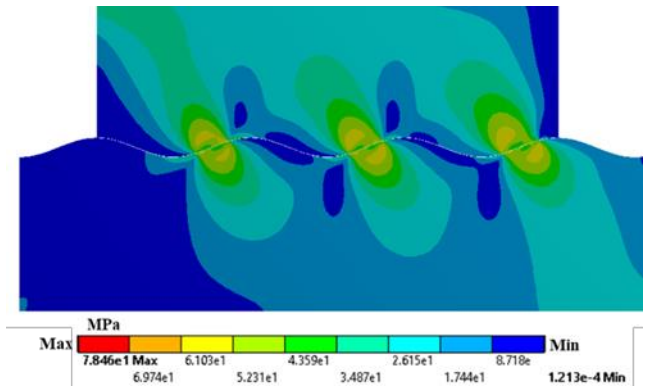


Fig. 6: Von Mises stress plot for a roughness with an amplitude of 1.5 μm and wavelength of 24 μm

Figure 7 shows the contact stress increase linearly with respect to the displacement in the x-direction U_x . This is because the deformation of the contact surface is in the linear elastic region as the maximum contact stress at $U_x = 0.1$ μm is lesser than the yield stress of 270 MPa as defined in table 1.

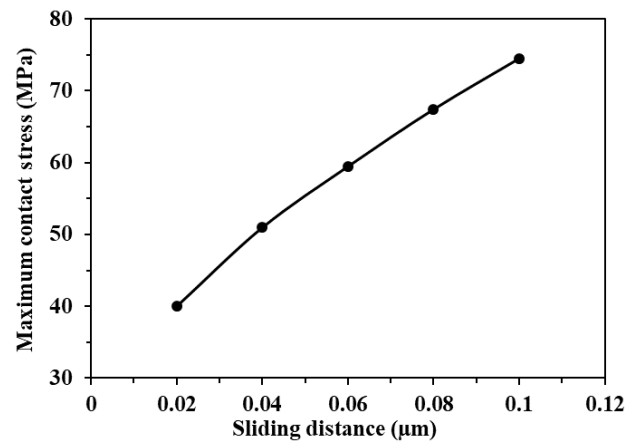


Fig. 7: The change in contact stresses with displacement in the x-direction

Figure 8 shows the change in contact area when we change the amplitude from 1 to 2 μm while keeping the wavelength constant at 24 μm. The results indicate that as the amplitude of asperity increase the contact area decrease. The contact area does not decrease linearly and seemingly plateau off at amplitude more than 1.8 μm. The contact stresses are higher when the contact area reduce. Figure 9 shows the change in contact area when we change the amplitude from X to Y μm while keeping the wavelength constant at 1.5 μm. As wavelength decreased, contact area decreased. Tan [13] performed finite element analysis of friction and actual friction tests and reported that the effect of contact area ratio

was more sensitive to friction than the effect of normal load. In this paper, the model with 1.5 μm amplitude and 18 μm wavelength showed higher shear stress than the model with 2.0 μm amplitude and 24 μm wavelength, which had smaller contact areas. Therefore, it is considered that the shear force is affected not only by the contact area but also by the surface shape.

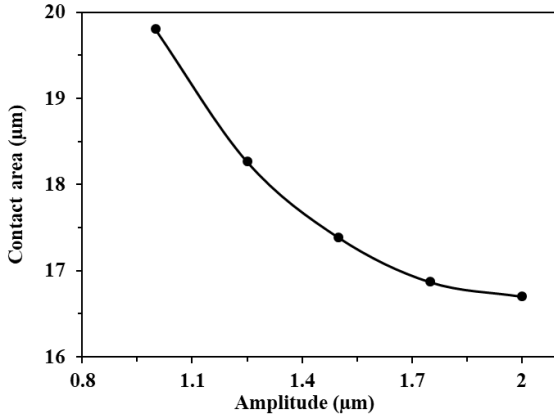


Fig. 8: Change in contact area with amplitude of asperity

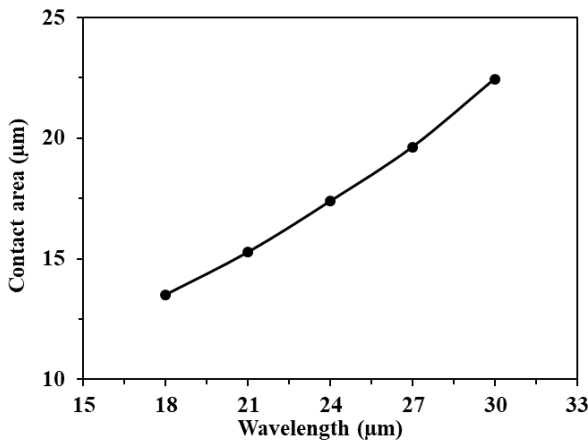


Fig. 9: Change in contact area with amplitude of asperity

3.3 Effect of Coefficient of Friction on Contact Stress

Figure 10 shows the change in maximum contact stress when we change the friction coefficient from 0.1 to 0.5 with the amplitude of 1.5 μm and the wavelength of 24 μm . As friction coefficient increased, maximum contact stress increased. Wang et al. [14] performed and analysed the forces and contact stresses generated during vehicle manoeuvring (free rolling, braking/acceleration, and cornering) with a three-dimensional (3D) tire–pavement interaction model using the FEM. The results showed that when the tire is free rolling or full braking, the vertical contact stresses are kept relatively constant as the friction coefficient increases. The tangential contact stress increases as the friction coefficient increases. When the tire is cornering, the contact stresses in three directions all increase as the friction coefficient increases. He guessed that this was probably because the deformation of the tire during cornering increased the maximum allowable friction before slipping. In this research, the maximum contact stress did not increase linearly, and the contact stress increased significantly when the coefficient of friction exceeded 0.3. If the normal contact

stress does not increase even when friction coefficient is higher, the tangential contact stress may tend to increase.

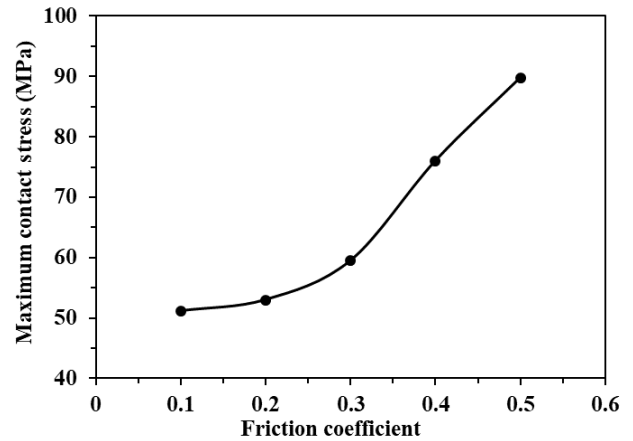


Figure 10 Change in normal contact stresses with friction coefficient

3.4 Effect of roughness on plastic deformation of 3D Surface

Figure 11 shows the initial stress state when the rough asperities comes in contact. The contact area for the rough asperities is significantly smaller compared to the smooth asperities, consistent with the findings in section 3.1. As a result, the contact stresses are higher for the rough asperities. Figure 12 shows the change in sliding distance with time for the rough and smooth asperities. The results show that the initial rate of displacement is slower for rough asperities due the large rate of plastic deformation. Subsequently, after the plastic deformation of the rough asperities, the upper body was able to displace at a higher rate.

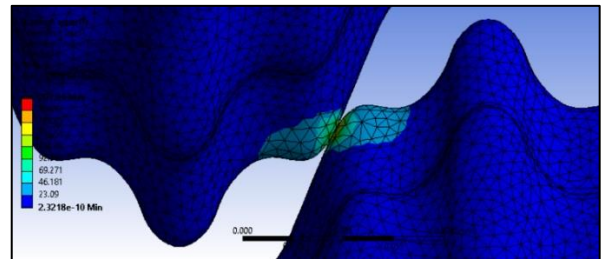


Fig. 11: Initial stress state when the rough asperity comes in contact

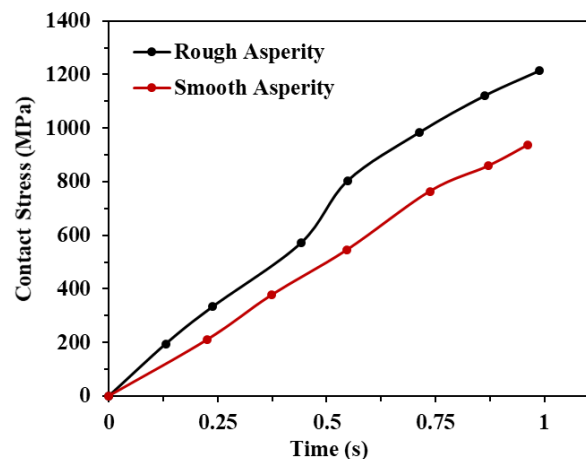


Fig. 12: The change in displacement in x-direction with time

4. CONCLUSION

In this research, we developed a 2D and 3D FEM to examine the effect of roughness on contact area, contact stresses and plastic deformation. In the 2D model, the surface roughness of contact surfaces was represented by idealised periodic sinusoidal wave. In the 3D model, the surface geometry was simplified from a typical fractal geometry using two different sinusoidal functions. Sensitivity analysis was conducted to determine the mesh size. We examine the effect of amplitude and wavelength of the idealised surface roughness on contact area. When the amplitude increased and wavelength decreased, the contact area decreased. Simultaneously, the magnitude of contact stresses increased. Contact stresses increase when we increase the coefficient of friction. Our results agree with the findings from [14]. The contact area for the rough asperities is significantly smaller compared to the smooth asperities. As a result, the rough asperities experience more plastic deformation.

ACKNOWLEDGEMENTS

The author would like to thank Professor Shaker A. Meguid and Mr. Lim for their help and support during the undertaking of the research at MADL University of Toronto, Canada. I would also like to thank JUACEP for supporting my stay at the University of Toronto.

REFERENCES

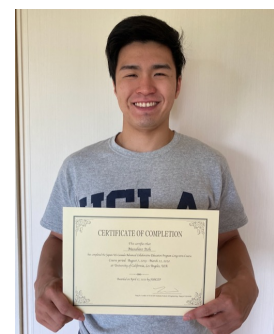
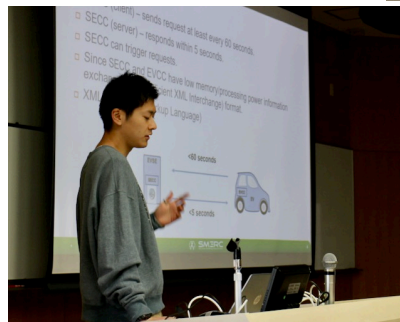
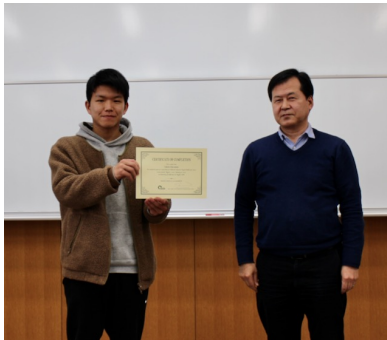
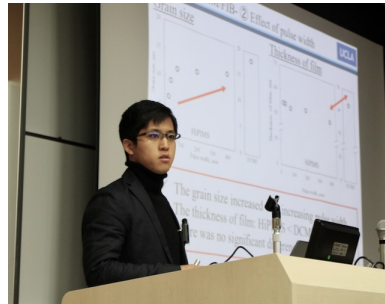
- [1] I. Hutchings and P. Shipway, *Tribology: Friction and wear of engineering materials: Second Edition*. 2017.
- [2] P. J. Blau, "The significance and use of the friction coefficient," *Tribol. Int.*, 2001.
- [3] "C. Stewart Gillmor. *Coulomb and the Evolution of Physics and Engineering in Eighteenth-Century France*. Princeton: Princeton University Press. 1971. Pp. xvii, 328. \$13.50," *Am. Hist. Rev.*, 1975.
- [4] K. J. Kubiak, T. G. Mathia, and S. Fouvry, "Interface roughness effect on friction map under fretting contact conditions," *Tribol. Int.*, 2010.
- [5] P. L. Menezes, Kishore, and S. V. Kailas, "Influence of roughness parameters on coefficient of friction under lubricated conditions," *Sadhana - Acad. Proc. Eng. Sci.*, 2008.
- [6] B. S. Ünlü and E. Atik, "Determination of friction coefficient in journal bearings," *Mater. Des.*, 2007.
- [7] S. Zhang, P. D. Hodgson, M. J. Cardew-Hall, and S. Kalyanasundaram, "A finite element simulation of micro-mechanical frictional behaviour in metal forming," *J. Mater. Process. Technol.*, 2003.
- [8] S. Zhang, P. D. Hodgson, J. L. Duncan, M. J. Cardew-Hall, and S. Kalyanasundaram, "Effect of membrane stress on surface roughness changes in sheet forming," *Wear*, 2002.
- [9] B. H. Lee, Y. T. Keum, and R. H. Wagoner, "Modeling of the friction caused by lubrication and surface roughness in sheet metal forming," in *Journal of Materials Processing Technology*, 2002.
- [10] H. Eid and G. G. Adams, "An elastic-plastic finite element analysis of interacting asperities in contact with a rigid flat," *J. Phys. D. Appl. Phys.*, 2007.
- [11] K. Komvopoulos and N. Ye, "Three-dimensional contact analysis of elastic-plastic layered media with fractal surface topographies," *J. Tribol.*, 2001.
- [12] W. Ramberg and W. R. Osgood, "Description of stress-strain curves by three parameters," *Natl. Advis. Comm. Aeronaut.*, 1943.
- [13] X. Tan, "Comparisons of friction models in bulk metal forming," *Tribol. Int.*, 2002.
- [14] H. Wang, I. L. Al-Qadi, and I. Stanciulescu, "Effect of surface friction on tire-pavement contact stresses during vehicle maneuvering," *J. Eng. Mech.*, 2014.

<3> Research Presentations

The 26th Students Workshop

For 2019 Medium- and Long-term Courses

Seven medium-term course students presented their research achievements and discussed with their Nagoya supervisors at the lecture room 241 on March 26, 2020. And a long-term student, who had been blocked participation in the workshop by the COVID-19 prevention measures, did his presentation on April 17.



The 26th JUACEP Students Workshop

Research presentations and discussions of JUACEP 2019 outbound participants

Date: Thursday, March 26, 2020 Venue: 241 Lecture room

Timetable

*10 minute-presentation + 4 minute-Q&A for each

Time	Name Adviser at NU	Presentation title	Adviser at US/Canada	page
9:45	Opening address by Prof. Yang Ju, JUACEP Leader			
9:50	Takeshi Matsumoto Assoc. Prof. K. Takagi Mechanical Systems Engineering	Toward Robust Tuning of Integral Resonant Control	Prof. Tetsuya Iwasaki Mechanical and Aerospace Engineering	Undisclosed
10:05	Takaaki Miyachi Prof. N. Umehara Micro-Nano Mechanical Science and Engineering	Finite Element Analysis of Contact in Asperities	Prof. Shaker Meguid Mechanical and Industrial Engineering	37
10:20	Takumi Kani Prof. N. Umehara Micro-Nano Mechanical Science and Engineering	Development of Low Adhesion Film Using Mesoporous Silica	Prof. Laurent Pilon Mechanical and Aerospace Engineering	39
10:35	Keita Umemura Assoc. Prof. K. Yamamoto Mechanical Systems Engineering	About ISO 15118	Prof. Rajit Gadh Mechanical and Aerospace Engineering	42
10:50	Break			
11:00	Yusaku Kawagoe Prof. T. Matsumoto Mechanical Systems Engineering	Conditional Machine Learning-Based Inverse Design of Photonic Metasurfaces	Prof. Aaswath Raman Materials Science and Engineering	Undisclosed
11:15	Tomoyasu Watanabe Prof. N. Umehara Micro-Nano Mechanical Science and Engineering	Effects of Pulse Width of VNB-TaMoW High Entropy Alloy Thin Films Deposited by HiPIMS	Prof. Suneel Kodambaka Materials Science and Engineering	Undisclosed
11:30	Completion Ceremony & Photography			
16:00	Tomohiro Saso Prof. N. Umehara Micro-Nano Mechanical Science and Engineering	Study of Tribological Performance of Aluminum Alloy 7075(T6)-TiB ₂ Nanocomposites	Prof. Xiaochun Li Mechanical and Aerospace Engineering	Undisclosed

Date: April 17, 2020

13:00	Masahiro Itoh Prof. K. Nagata Aerospace Engineering	The Wind Tunnel Experiment of Low Profile Double Floating-Elements Shear Stress Sensor	Prof. Chang-Jin Kim Mechanical and Aerospace Engineering	45
-------	---	---	--	----

Finite Element Analysis of Contact in Asperities

University of Toronto, Canada
Department of Mechanical and Industrial Engineering
Takaaki Miyachi
Supervisors: Shaker A. Meguid

0

Background

Friction in sliding and rotating parts of machines

Energy loss

Fretting

Fatigue failure

Low friction is essential

Important to assess and determine the parameters that governs the mechanical properties of contact surfaces

1

Previous study

The effect of friction is dependent on many factors
- Surface roughness, contact area, relative speed...etc

Study of friction coefficient of journal bearing ^[1]

Load and velocity increases

Friction coefficient increases

[1] B. S. Önlü and E. Atik, "Determination of friction coefficient in journal bearings," Mater. Des., 2007

2

Previous study

FEM friction analysis

- The roughness of contact surfaces decreases during sliding
- Local contact pressure is much higher than mean contact pressure due to the variation of actual contact area

[2] S. Zhang, P. D. Hodgson, M. J. Cardew-Hall, and S. Kalyanasundaram, "A finite element simulation of micro-mechanical frictional behaviour in metal forming," J. Mater. Process. Technol., 2003

3

テキスト

Objective

Zhang didn't change surface shape and roughness
In our research,...

Analyze the effect of surface shape and roughness on contact asperities

Objective

Study effect of amplitude and wavelength of asperity on the contact area

2D model

Surface roughness → Idealized period sine wave

4

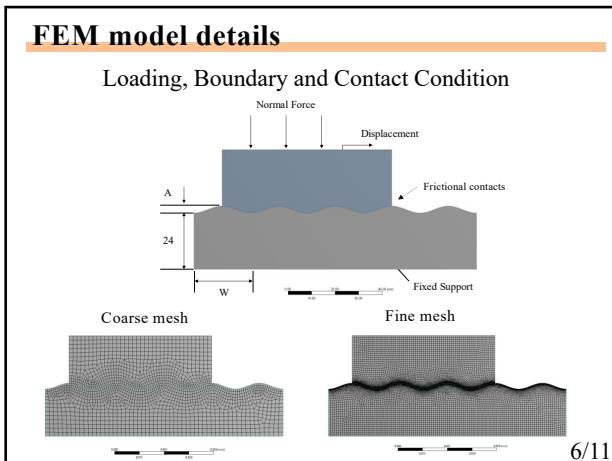
FEM model details

Material Properties of austenitic stainless steel [3]

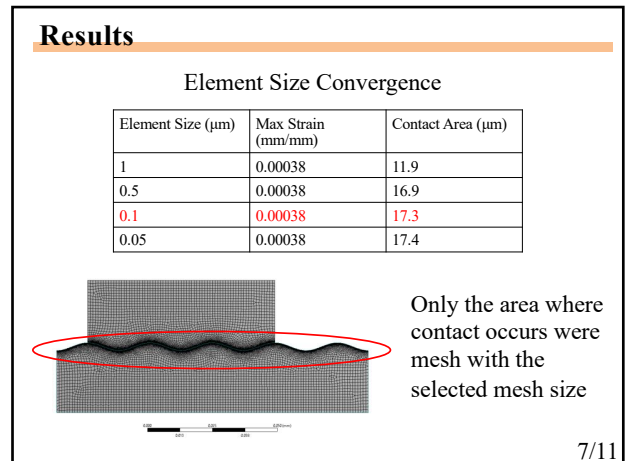
Properties	Values
Young's Modulus (GPa)	207
Poisson's Ratio	0.3
Yield Stress (MPa)	270

[3] W. Ramberg and W. R. Osgood, "Description of stress-strain curves by three parameters," Natl. Adv. Comm. Aeronaut., 1943

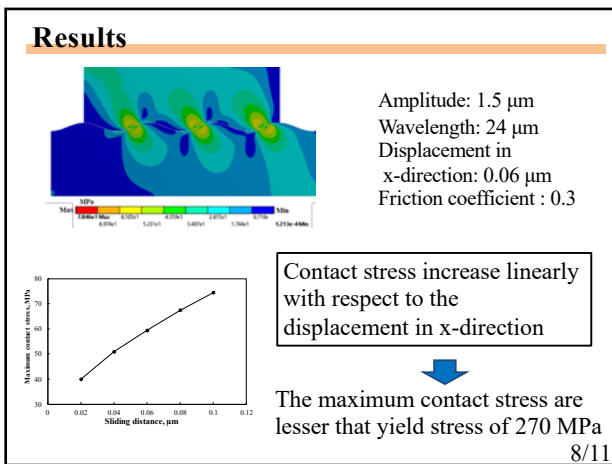
5



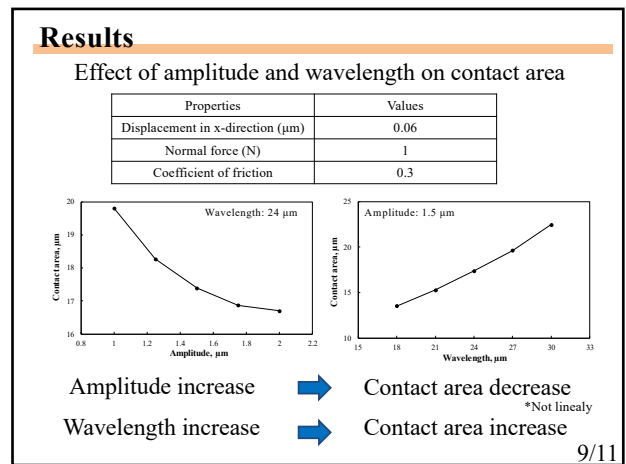
6



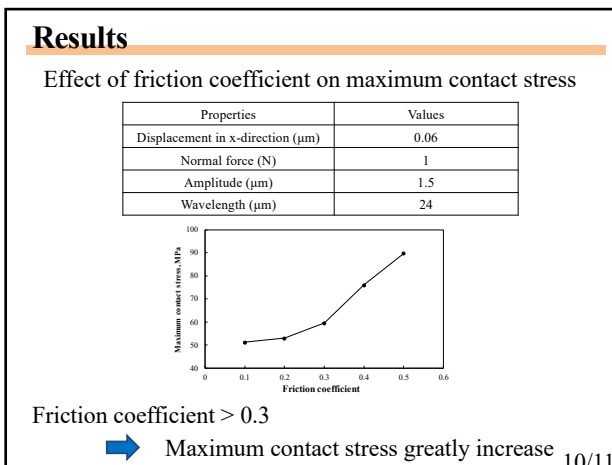
7



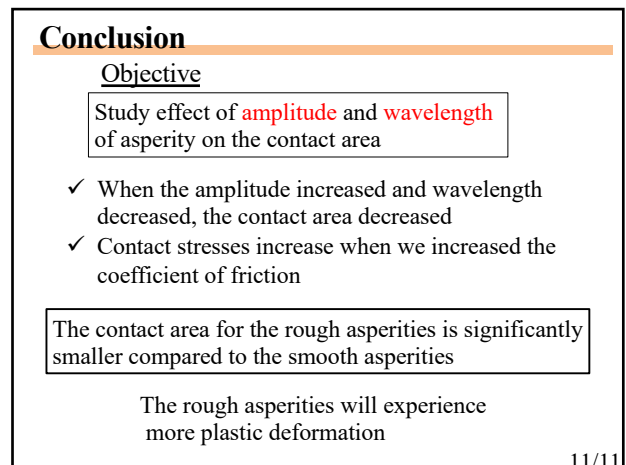
8



9



10



11

Development of low adhesion film using mesoporous silica

University of California, Los Angeles
Mechanical And Aerospace Engineering
Visiting Graduate Researcher
Takumi Kani

0

Motivation

low adhesion film

SLIPS

- ✓ Liquid and ice repellency
- ✓ Self healing
- ✓ Pressure stability

Tak-Sing Wong, et al. "Biomimetic self-repairing..."
Nature, 477, 443-447 (2011)

1

SLIPS (slippery liquid infused porous surface)

The necessary conditions for SLIPS

1. Lubricating liquid must wick into, wet and stably adhere within the substrate.
2. Mesoporous solid must be preferentially wetted by the lubricating liquid rather than by the liquid one wants to repel.
3. Lubricating and impinging test liquids must be immiscible.

Wenzel : Gets wet and spread easily.
Cassie-Baxter : Increased contact angle with air.
SLIPS : Use lubricating oil instead of air.

Tak-Sing Wong, et al. "Biomimetic self-repairing slippery..."
Nature, volume 477, pages 443-447 (2011)

2

Material used for SLIPS

Kind of porous solid : Mesoporous silica film

- ✓ simple synthesis
- ✓ easily controlled structural properties

Type of lubricating oil : PFC (perfluorocarbon) GPL 106

- ✓ Omniphobic properties
- ✓ High density

3

Previous research

How to make SLIPS
Prepared by introducing silicone oil into porous TiO2 nanoparticle coating

LFS(Liquid Flame Spray)+Oil(SLIPS) showed

- excellent anti-icing properties
- Good hydrophobic

Paxton Juari, et al. "Achieving a slippery..."
Applied Physics Letters 110, 16 (2017)

4

Experimental procedure

- Contact angle θ_c

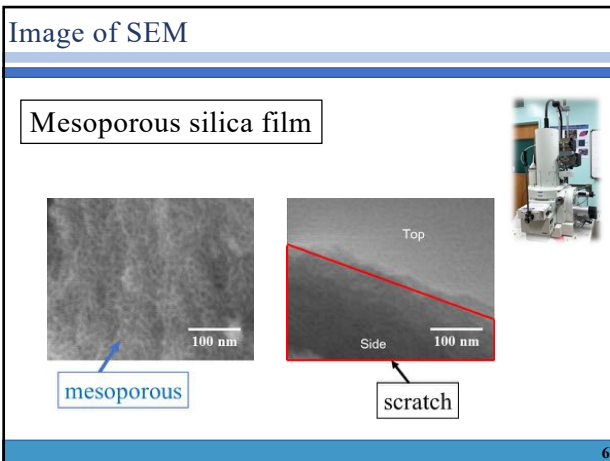
θ_c : large
- Water sliding angle θ_s

θ_c : small

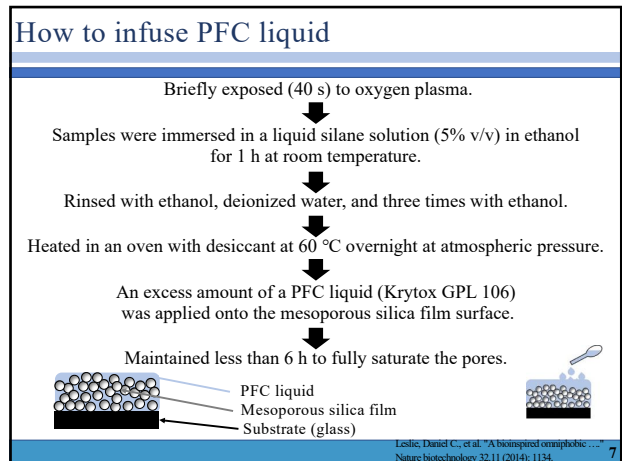
θ_s small

large

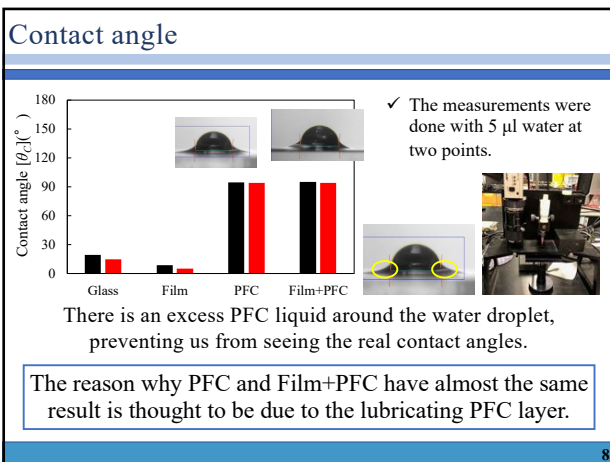
5



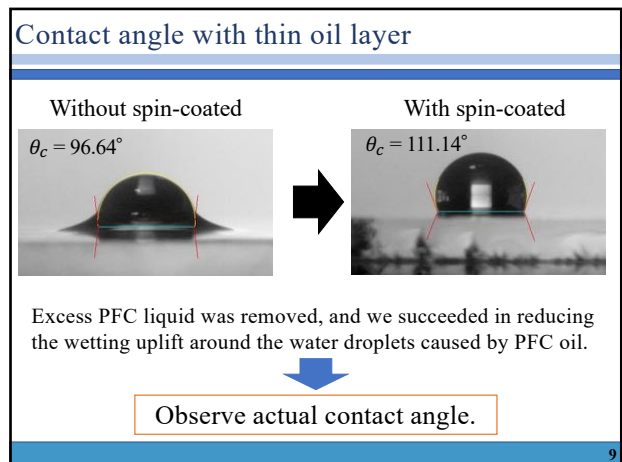
6



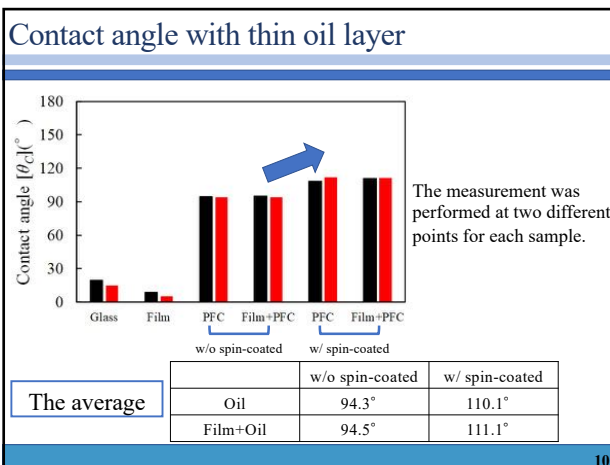
7



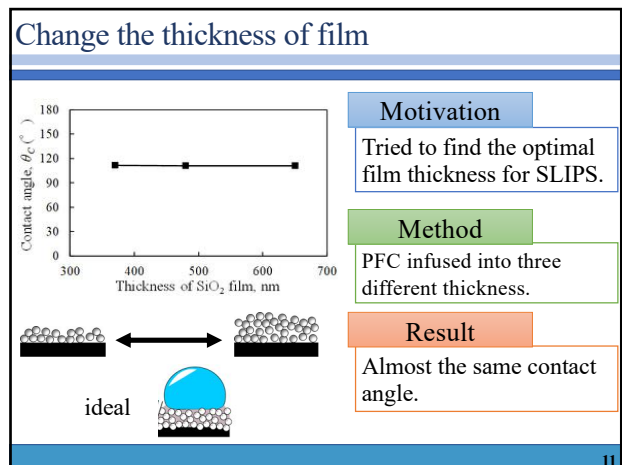
8



9



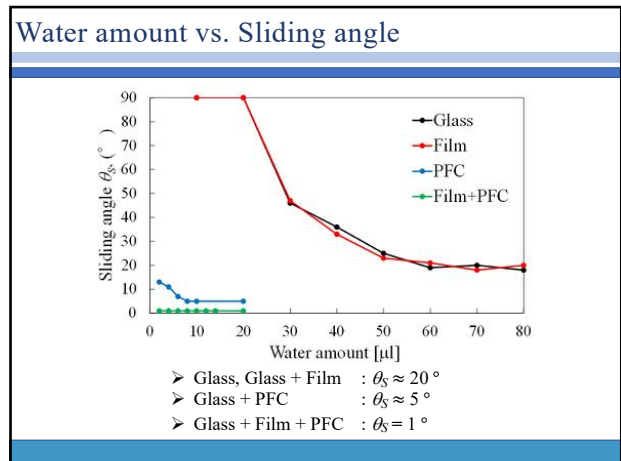
10



11

Device for sliding angle

12



13

About PFC

PFC

$\theta_c = 94.50^\circ$

Good

$\theta_S \approx 5^\circ$

4 μl

$\theta_S = 11^\circ$

Bad

8 μl

$\theta_S = 5^\circ$

Sometimes, water droplet slide maintaining high contact angle, but sometimes it spread on the way, as shown on the right picture.

We had to add PFC for each experiment because water droplet was easy to spread when repeated.

↓

There is a problem with stability.

14

About film+PFC

Film+PFC

$\theta_c = 96.64^\circ$

$\theta_S = 1^\circ$

2 μl, $\theta_S = 1^\circ$

- ✓ Excess PFC liquid makes small amount of water droplet slide.
- ✓ SLIPS has good sliding angle than Glass + PFC.

Very slowly, but the water droplet slid at 1° .

■ All experiments were performed with the same sample, but high contact angle was maintained.

15

Change the thickness of film

Motivation

Tried to find the optimal film thickness for SLIPS.

Method

PFC infused into three different thickness.

Result

All the same sliding angle ($\theta_S = 1^\circ$).

There is no influence of thickness of mesoporous film.

16

Conclusion

Conclusion

- ◆ I made SLIPS using mesoporous silica film.
- ◆ I measured the contact angle of 4 samples.
- ◆ I designed and made the device of measuring sliding angle.
- ◆ I measured sliding angle.

Future work

We need to measure ice adhesion strength.

17

About ISO 15118

Umemura Keita
26th December 2020

SMERC

1

What is ISO 15118?

- Standard that governs the communication between
 - EVCC (Electric Vehicle Communication Controller) that is within the EV.
 - SECC (Supply Equipment Communication Controller) that is within the EVSE (EV Supply Equipment), i.e., the charger.

SMERC

2

Communication between EV and EVSE

Communication Standard	Physical Interface	Communication signals	Provide SOC	DC/AC charging	V2G capability	Popularity
SAE J1772	CCS Combo	PWM	No	Both	No	High
CHAdeMO	CHAdeMO	CANbus	Yes	DC	Yes	Low
ISO 15118	CCS Combo	Power line	Yes	Both	Yes	High

Characteristics of various charging standards

- EVSE - EV Supply Equipment
- PWM - Pulse Width Modulation
- CCS - Combined charging system
- CAN - Control Area Network
- SOC - State of Charge
- V2G - Vehicle to Grid

EV charging station connectors

SMERC

3

Client server protocol

- EVCC (client) – sends request at least every 60 seconds.
- SECC (server) – responds within 5 seconds.
- SECC can trigger requests.
- Since SECC and EVCC have low memory/processing power information exchange in EXI (Efficient XML Interchange) format.
- XML (Extensible Markup Language)

SMERC

4

ISO 15118 characteristics

Schematic with EV, EVSE and their respective controllers

- EVSE – EV Supply Equipment
- EVCC – EV Communication Controller
- SECC – Supply Equipment Communication Controller

Secure	Supports V2G
Ease of payment	Supports AC and DC charging
Supports inductive charging	Optimal use of energy resources

SMERC

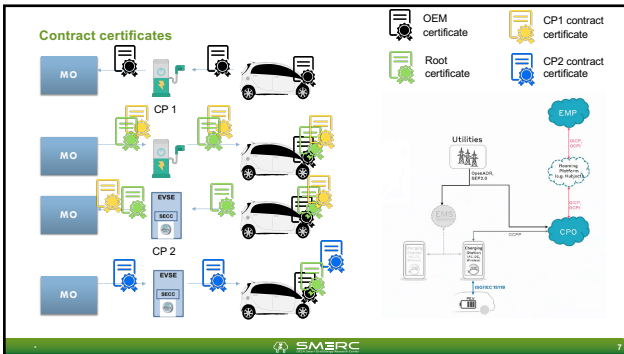
5

Certificates

- X.509 certificate – Not a text file.
- File format .cer, .pem, .crt etc.
- X.509 is a standard for public key infrastructure – necessary to create, store and distribute certificates securely.
- EV can hold 10 certificates at a time.
- Provisional certificate by Original Equipment Manufacturer (OEM).
- Mobility operator (MO) installs “root certificate” via EVSE.
- MO also installs contract certificates for different charge point providers via EVSE.
- Ensures that there is no need to pay by card, cash etc.

SMERC

6



7

Messages between EV and EVSE

- EXI format (Efficient XML Interchange) – Binary data format
- Compresses request messages to 10% of size and response to 5.5%
- Decreases storage requirements and increases read speed.
- Hash algorithms for XML signatures.
- Lower computing time and power

8

Steps

- Depends on communication level between EV and EVSE.
- Fewer possibilities if either lack high level communication ability.
- High level communication required for identification, payment, load leveling etc.
- Basic signaling sufficient for initializing charging, identifying vehicle status.

A	Start of charging process
B	Communication setup
C	Certificate Handling
D	Identification, Authentication and Authorisation
E	Target setting and charge scheduling
F	Charge controlling and Re-scheduling
G	Value-added services
H	End of charging process

9

A – Start of charging & B – Communication setup

- A – Start of charging
 - Connect cable between EV and EVSE.
 - EVSE sends PWM duty cycle that is interpreted by EV.
- B – Communication setup
 - EVCC sends first high level signal to SECC.

A	Start of charging process
B	Communication setup
C	Certificate Handling
D	Identification, Authentication and Authorisation
E	Target setting and charge scheduling
F	Charge controlling and Re-scheduling
G	Value-added services
H	End of charging process

10

C – Certificate handling

- Replace invalid/expired certificate with new certificate from SA.
- EVCC requests update providing SA info.
- SECC asks SA for certificate update.
- SECC updates certificate in EV.
- If no certificate, EV identified with OEM provisioning certificate installed during EV production.
- SECC can send certificate to all possible SA to obtain required certificate.
- ISO 15118 does not specify requirements to pay by card/cash.

A	Start of charging process
B	Communication setup
C	Certificate Handling
D	Identification, Authentication and Authorisation
E	Target setting and charge scheduling
F	Charge controlling and Re-scheduling
G	Value-added services
H	End of charging process

11

D- Identification and authorization

- EVCC triggers initialization of authorization.
- SECC and EVCC exchange ID (EVSE ID and Contract ID).
- Both IDs maybe forwarded to SA for validation.
- User could also type in some ID in HMI (Human Machine Interface) on EVSE which maybe sent to SA.
- Session ID defined and process can start (charge/discharge/other)

A	Start of charging process
B	Communication setup
C	Certificate Handling
D	Identification, Authentication and Authorisation
E	Target setting and charge scheduling
F	Charge controlling and Re-scheduling
G	Value-added services
H	End of charging process

12

E – Target setting and charge scheduling

- SECC and EVCC exchange max current limitations.
- If user inputs min SOC required at departure - SA can propose charging schedule to SECC based on power limits, local generation, sales tariff table etc. or SA sends information to SECC and then either SECC or EVCC generates schedule.
- In case of DC charging, max possible power is sent.

A	Start of charging process
B	Communication setup
C	Certificate Handling
D	Identification, Authentication and Authorisation
E	Target setting and charge scheduling
F	Charge controlling and Re-scheduling
G	Value-added services
H	End of charging process

SMERC 13

13

F- Charge controlling and re-scheduling

- EVCC sends SECC the current status.
- EVCC signs meter information from SECC.
- SECC sends signed meter info to SA.
- Charge rescheduling occurs if changes in info from SA (like local load change). SECC interrupts schedule and new schedule based on E.
- Charge reschedule also if user changes departure time or energy required.

A	Start of charging process
B	Communication setup
C	Certificate Handling
D	Identification, Authentication and Authorisation
E	Target setting and charge scheduling
F	Charge controlling and Re-scheduling
G	Value-added services
H	End of charging process

SMERC 14

14

F- Charge controlling and re-scheduling

- Reactive power compensation
 - EVCC indicates reactive power compensation is possible.
 - SECC requests reactive power compensation of certain value.
- V2G support
 - EVCC indicates V2G possibility, max rate of power discharge and energy given considering user constraints.
 - SECC requests V2G and provides grid schedule which EVCC can accept/reject.

A	Start of charging process
B	Communication setup
C	Certificate Handling
D	Identification, Authentication and Authorisation
E	Target setting and charge scheduling
F	Charge controlling and Re-scheduling
G	Value-added services
H	End of charging process

SMERC 15

15

G- Value added services & H- End of charging process

- G – Value added services
 - User requests information like pre-booking chargers, estimating energy required for journey etc., this is sent from the SECC to the EVCC.
 - Battery status and state of charging can be provided to SECC or SA from EVCC. EVCC can decline.
- H – End of charging process
 - User can request end of charging process on EV or EVSE side. Hence, EVCC will request SECC to stop charging or SECC directly stops.


A	Start of charging process
B	Communication setup
C	Certificate Handling
D	Identification, Authentication and Authorisation
E	Target setting and charge scheduling
F	Charge controlling and Re-scheduling
G	Value-added services
H	End of charging process

SMERC 16

16

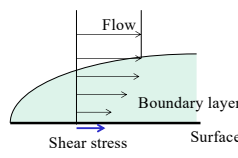
THE WIND TUNNEL EXPERIMENT OF LOW PROFILE DOUBLE FLOATING-ELEMENTS SHEAR STRESS SENSOR

Masahiro Itoh
 Department of Mechanical and Aerospace Engineering, University of California, Los Angeles
 Micro and Nano Manufacturing Laboratory
 Prof. Chang-Jin Kim




1

Measuring shear stress



Measuring shear stress

- Important for friction drag evaluation of transportation equipment
- A challenging attempt




2

Methods for measuring shear stress

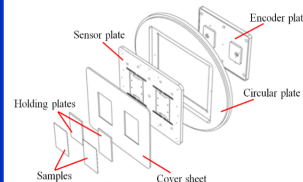
Shear stress sensor	
Indirect method	Direct method
Pro...High reactivity, sensitivity Con...Low accuracy (need assumptions) • Hot-film sensor	Pro...High accuracy Con...Complex structure • Floating element sensor

A direct shear sensor with double floating elements has been developed for hydrodynamic applications in Professor CJ Kim's lab at UCLA. A previous JUACEP student showed this sensor can be used for aerodynamic flows in a wind tunnel. I confirmed the previous results and further characterize the sensor in airflow.

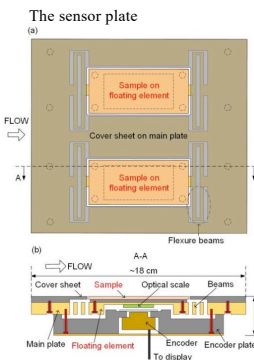



3

Sensor structure

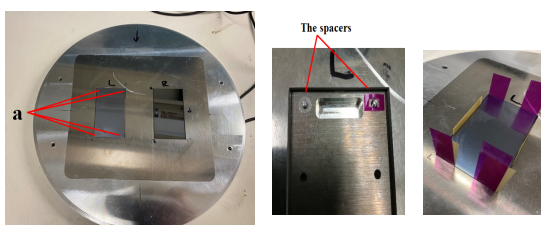


The sensor plate





4

Installing sample



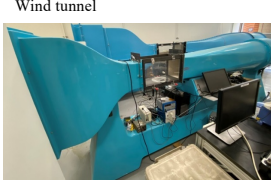
Need to put spacers between floating element and sample at point a in order to adjust sample height and between sample and cover sheet in order to make enough gap so that sample can move.



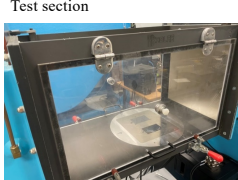
5

Wind tunnel experiment


Wind tunnel



Test section

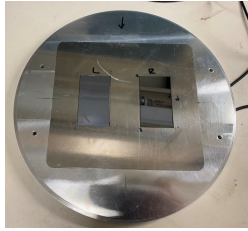


- The sensor measures the average of shear stress
- Experiment is repeated 4 times
- In laminar-turbulent transition
- Velocity: every 5m/s (5m/s ~ 30m/s) and every 2.5m/s (30m/s ~ 40m/s)



6

Experiment with two smooth surfaces

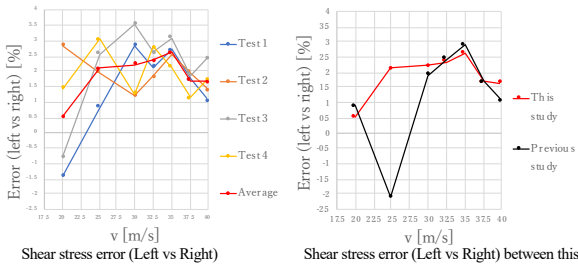


The displacement of floating element at 0~15m/s is so small that it is much affected by vibration of the sample. The value of shear stress at these velocity doesn't have credibility.

AMICRONAN manufacturing

7

Experiment with two smooth surfaces



Shear stress error (Left vs Right)

Shear stress error (left vs right) [%]

Shear stress error (Left vs Right) between this study and previous study

Shear stress error of this study: 0.5~2.6%
previous study: -2.1~2.9%

Repeatability of the shear stress error was confirmed

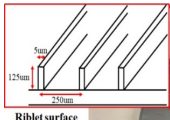
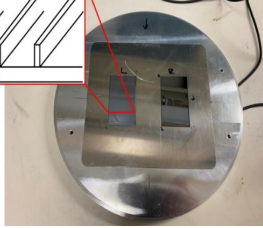

AMICRONAN manufacturing

8

Experiment with a riblet and a smooth surface

Riblet

The structure with regular groove
Previous studied have shown that blade riblet would gain the highest drag reduction.

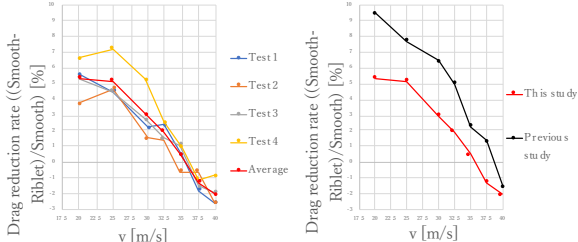
Riblets surface

Damaged surface

AMICRONAN manufacturing

9

Experiment with a riblet and a smooth surface



Drag reduction rate ((Smooth-Riblet)/Smooth) [%]

Drag reduction rate ((Smooth-Riblet)/Smooth) [%]

Drag reduction rate ((Smooth-Riblet)/Smooth) between this study and previous study

- The drag reduction of this study is less than that of previous study.
- The highest drag reduction rate was at the velocity of 20m/s in both studies, and the drag reduction rate decreased with velocity in both studies.

AMICRONAN manufacturing

10

The effect of the sensor's natural vibration caused by airflow

The sensor haven't been originally developed for aerodynamic flows. It is possible that the sample's displacement is effected by the sensor's natural vibration caused by airflow and shear stress value is changed.

Removed the sensor's natural frequency from data the sensor measured by using band pass filter

Result:

The sensor's natural frequency caused by airflow is quite small compared to resonance frequency.
No need to consider airflow effect to the value of measured shear stress that the sensor measured.

AMICRONAN manufacturing

11

Conclusion

Although I couldn't reach same drag reduction rate as a previous study's data in experiment with a riblet and a smooth surface because of damage on the riblet surface, I confirmed the repeatability of the shear stress error.

I confirmed this floating element sensor can be used and characterized it for aerodynamic flows.

AMICRONAN manufacturing

12

<4> Findings through JUACEP

- Students' reviews ...49
- Questionnaires (in Japanese) ...57

My treasure memory

Name: Umemura Keita

Affiliation at Nagoya University: Mechanical Systems Engineering

Participated program: Medium course 2019

Research theme: About ISO 15118

Advisor at the visiting university: Prof. Rajit Gadh

Affiliation at visiting university: Mechanical & Aerospace Engineering at UCLA



The all experiences in the JUACEP were wonderful. I did research under the Professor Rajit Gadh. I was concerned whether I could do research well in UCLA because of language difference. But the laboratory members were very kind. When I had a problem, they always helped me. Without their helps, I must not finish my research. I appreciate very much.

In holiday, I went to a lot of places in Los Angeles. The all places –Santa Monica, Down Town, Hollywood, Baseball Stadium- are very moving. Especially, the most favorite place is art museum. Before I come to Los Angeles, I have never been to art museum. But the atmosphere of the Los Angeles made me want to go to a new place. When I looked into the museums in Los Angeles, I found that all museums were very popular and famous around the world. So I went to the all museums in Los Angeles. I had no knowledge about artwork, it was very interesting to walk around in the museum. There are many artworks by famous painter, for example Picasso, Monet, Gogh and so on.

All experience in these 6 months must be treasure in my life. I absolutely recommend this program to anyone who is interested in.



Findings through JUACEP

Name: Takumi Kani

Affiliation at home country :

Dept. of Micro/Nano Mechanical Science of Engineering, Nagoya Univ.

Participated program: Medium course

Research theme: Development of low adhesion film using mesoporous silica

Advisor at the visiting university: Prof. Laurent Pilon

Affiliation at visiting university: Department of Mechanical and aerospace engineering, University of California, Los Angeles



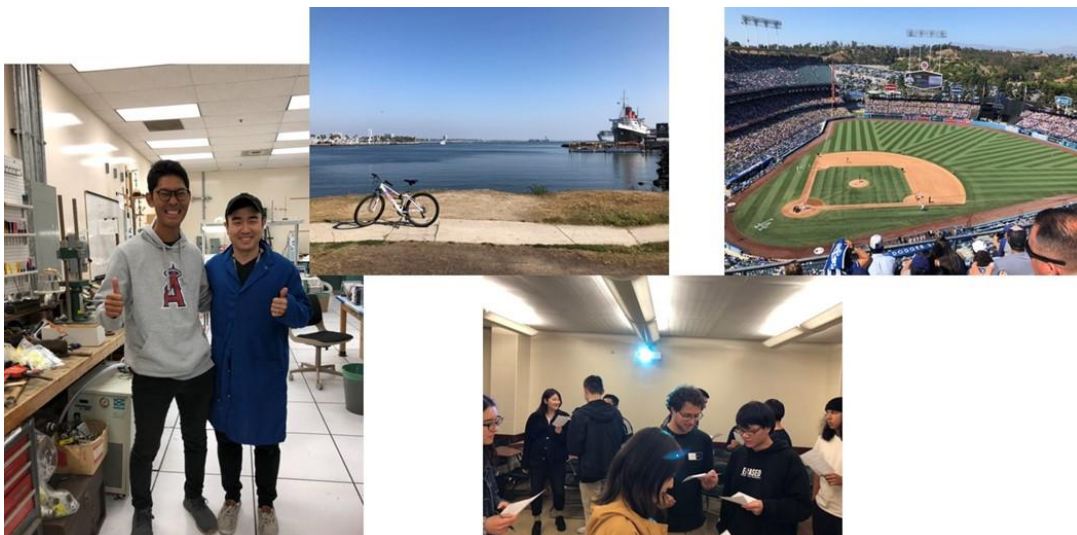
I got a lot of wonderful experiences in the U.S through JUACEP program. Before I came, I was worried about university and daily life. Because it was first time to live in foreign country. However, I realized that the concern was completely unnecessary. People I met in the U.S are very kindly and friendly. Through this study abroad, I was able to touch kindness across borders.

I would like to introduce my research life at UCLA. The field of research in Prof. Pilon is different from my research in Japan. So I thought that I would join the project of Prof. Pilon group. However, when I told him about my research in Japan, he designed a research theme that would be relevant to research in Japan and the U.S. My research at UCLA is a kind of development and evaluate thin film and lubricant oil. Since this theme was a joint research with a chemical laboratory, students who belong to chemical laboratory taught me how to handle equipment and make samples. The laboratory I belong to was composed with students from various countries such as France and Colombia. This research experiences with students from different majors changed the view of thinking for the research.

I participated in a club of gathering students interested in Japanese culture. This club is held once a week at the university, discuss each other's culture and interests using both Japanese and English. Many of them were interested in Japanese comics and music, I really felt that Japanese culture was spreading all over the world.

I think it was very good that I bought a bicycle in the U.S. I bought a bicycle for going to school because the house where I lived was far from to the university. As a result, this purchase was very good because the range of action became wide and I could go to various places with bicycle. There are many sunny days in Los Angeles and I was able to spend comfortably by bicycle. It was great to be able to go to the watching sports game that I wanted.

I am very appreciated with all of the people who met and supported me.



Findings through JUACEP

Name: Yusaku Kawagoe

Affiliation at Nagoya University: Mechanical Systems Engineering

Participated program: Medium course 2019

Research theme: Conditional Machine Learning-Based Inverse Design of Photonic Metasurfaces

Advisor at the visiting university: Prof. Aaswath Raman

Affiliation at visiting university: Materials Science and Engineering - UCLA



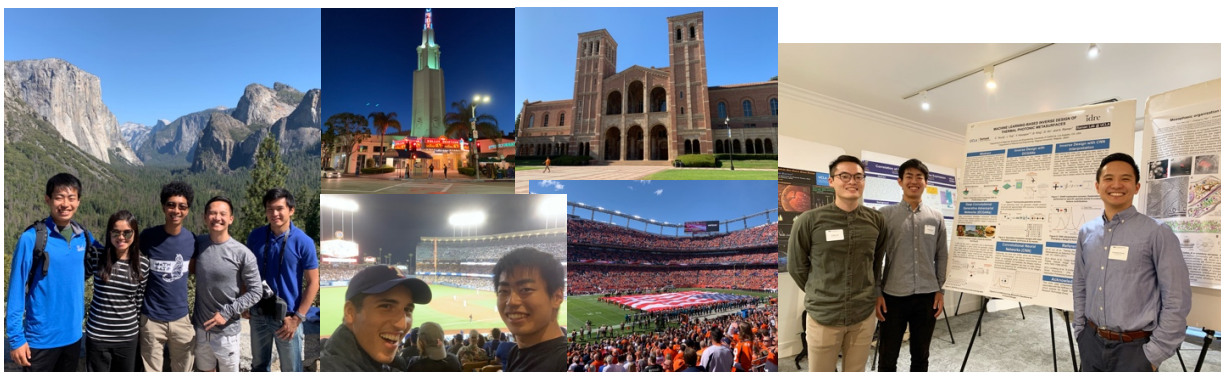
My life in LA for six months has been the most exciting and memorable experience of my life. UCLA, where people from all regions of the world such as Europe and Asia gather, gave me a wonderful opportunity to learn about these differences in cultures and expand my vision. I developed proficiency in sophisticated technological expertise, and expanded my skillset through conducting research in a challenging and distinctly different environment from Japan.

A few of the highlights of studying at UCLA include learning machine learning, various kinds of simulation, and data analysis under the supervision of Professor Raman. As part of a three-member project team, I helped develop a program to generate images based on user-defined conditions using a machine learning technique called GAN (Generative Adversarial Network). GAN is one of the applications of artificial intelligence (AI) in the world today that can be used in a wide range of industries, such as automobiles, pharmaceuticals, medicine, architecture, etc. We applied this method to the design of nanophotonic devices that absorb electromagnetic fields. My contributions toward this project during my time at UCLA may contribute towards two publications that are currently pending review. I plan to use the AI experience that I have acquired at UCLA to my research at Nagoya University.

In addition to the technical skills, I gained unforgettable, precious friendships with my lab members. They were not only smart and friendly, but also they exhibited professional charisma. They invited me to a hike on my first weekend in LA and we soon became friends. We played board games at my friend's house, trained at the UCLA gym, enjoyed the all-you-can-eat dining halls, and explored restaurants near UCLA. I became best friends with Chris, a Ph.D. student in Professor Raman's lab and the project leader. He taught me not only the techniques related to research, but also various philosophies about work and life. I am convinced that being able to absorb American philosophy and culture will have a significant impact on my future career. I had a farewell party on my last day in LA. Although I really miss them, I am confident our paths will cross again someday.

On weekends, I traveled to national parks and cities in various states. Every trip has given me a new experience. On my travels, I had many encounters, such as making friends with people from different states. I was impressed by the superb view of America's natural landmarks and I felt how small I am. Solving unexpected big and small problems while traveling made me stronger. My most memorable experience is hiking at Yosemite National Park with my lab members.

Finally, I would like to thank Professor Aaswath Raman and all the lab members for giving me such a wonderful opportunity to study in Raman Lab. I also really appreciate JUACEP for providing me with this extraordinary opportunity.



Improving my personality through JUACEP

Name: Tomohiro Saso

Affiliation at Nagoya University: Micro-nano Mechanical Engineering

Participated program: Medium course 2019

Research theme: Study on tribological performance of aluminum alloy 7075(T6)-TiB₂ nanocomposites

Advisor at the visiting university: Prof. Xiaochun Li

Affiliation at visiting university: Mechanical and Aerospace Engineering, UCLA



First, about my research. I joined the laboratory that was doing research about enhancing metals' mechanical properties, which was slightly different from what I had been studying in Japan. Although I didn't know so much for the metal side, everyone in the lab treated me so nicely that I soon got used to the situation. Many PhD. students participated in that lab. I was very impressed by their passion toward the research. Scheduling the procedure, preparing samples on time, deeply think of the mechanisms that may concern, and so on. These techniques can surely be used for the rest of my master's research and also for a job. During my stay in UCLA, I put my effort on research the most throughout my life. The opportunity of having this experience I would have never had in Japan is the most valuable thing I conclude.

Second, about the life in Los Angeles. I felt the complete difference of personalities between Americans and Japanese. Americans are talkative, express their thoughts to others without hesitation which lead to easiness to be friends each other. On the other hand, most Japanese are relatively quiet, tend to avoid any kind of trouble. Since these differences of personalities between people in two countries, I was very stimulated through my stay in the U.S. Specifically, in Japan, I was not willing to talk with strangers, but by the end of my stay in the U.S., I had no hesitation to talk with people who I first met; For example, shoppers and staffs in a supermarket, people in a bus, or even people just walking on the streets. By communicating with people more frequently, it became easier for me to solve and prevent troubles or misunderstandings which save more time, and able to get new knowledge that I didn't expect before talking.

Also, I learned that arguing about problems which one cannot tolerate is very important to live in the U.S. For example, one day I got my flight time rescheduled from night to morning on the same day. With that schedule, I couldn't be on flight time, so I complained to the airplane company and they easily and kindly rebooked the flight which departs at night for free. Different from the Japanese company, they take our opinion into account only when we argue, otherwise it would be us which lose the opportunity. Another skill I learned to live in the U.S. is to take care of oneself. During Thanksgiving holidays in December, I got my bike stolen from the balcony of my house because I was out for a trip. It is so pity, but after all, I should have known that there are some crazy people in LA who are always looking for bike to steal. I needed to keep the bike in my room at least during the trip. Any unbelievable things happen in LA compared with Japan, so everybody need to be aware of dangerousness of living in LA, and it is their own responsibility to stay safe.



Precious experience in the United States

Name: Takeshi Matsumoto

Affiliation at Nagoya University: Mechanical Systems Engineering

Participated program: Medium course 2019-2020

Research theme: Toward robust tuning of Integral Resonant Control

Advisor at the visiting university: Prof. Tetsuya Iwasaki

Affiliation at visiting university (Dept & Univ): Engineering, UCLA



My six months stay in U.S was my first challenge. I was born and raised in Japan and had lived with my family in whole my life. As most Japanese are said conservative, I was also one of the typical Japanese. I hesitated to study and live other places away from where I was. However, I realized that my horizons and what I experienced so far were totally narrow when I was traveling the other countries for three weeks. At the same time, I wanted to know about other cultures and what the people who were born and raised in the community believe. Having those thoughts, I decided to join the JUACEP. As a result, I am totally satisfied with my six months stay and made the right decision.

Research in UCLA

I joined the laboratory of Prof. Iwasaki in mechanical engineering of UCLA and researched about control engineering. I faced some difficulties in first several weeks. Thankfully, he offered many helps to me and I was able to conduct research without any concern. I learned not only deep knowledge which is related to my major but also differences how to conduct our research between Japanese and American laboratory. I am going to leverage it for my future work and convey good things of American laboratory to people around me. I am sure that what I experienced during my six months stay is going to make me a greater engineer.

Life in Los Angeles

Firstly, I was very nervous because this stay was the first time to live away from my family. But all my worries were gone right away. Fortunately, my roommates and lab mates helped me in every situation and made me excited in the U.S life without any problem. I could know both light and dark of the United States. Technologies are advanced such as electrically-powered cars and solar power. On the other hand, I observed the huge gap between rich and poor. I found that we have to consider carefully when we adopt American systems.



Thank you for your support!!!

Findings through JUACEP in UCLA

Name: Tomoyasu Watanabe

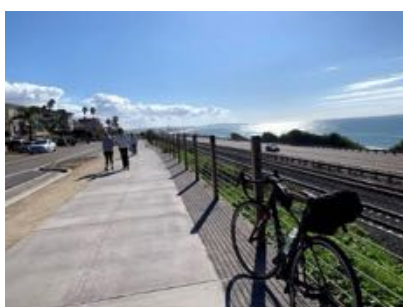
Affiliation at Nagoya University: Department of Micro-Nano Mechanical Science and Engineering

Participated program: Medium course 2019

Research theme: Effects of Pulse Width of VNbTaMoW High Entropy Alloy Thin Films Deposited by HiPIMS

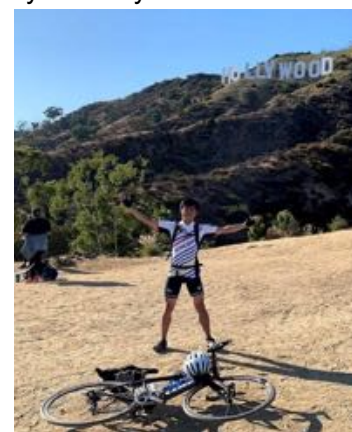
Advisor at the visiting university: Prof. Suneel Kodambaka

Affiliation at visiting university (Dept & Univ): Department of Materials Science and Engineering, University of California, Los Angeles



I experienced various special events through JUACEP. I would like to introduce two events that are particularly impressive. The first is regarding a bike. I brought my bike from Japan with my other luggage. I used my bike not only for commuting to UCLA but also for everyday shopping and sightseeing. In Los Angeles, it's really good for cyclists because it doesn't rain much as compared to Japan (only about 10 days in the last 6 months). Of course, we can use buses and trains in Los Angeles, however they are much worse than that in Japan. The delay of more than 10 minutes was common, and there were several times that the bus passed without stopping when I was waiting at bus stop. Many people (including homeless and drug addicts) use these public transportations, so it was a bit dangerous at times. I cycled to various locations, including Santa Monica Beach, Hollywood Sign, Malibu Beach, etc. One of the most memorable trips is riding my bike alone from Los Angeles to Mexico via San Diego at the end of year. Cycling approximately 260 km in two days was very tough, but I could cycle on the freeway (highway in Japan) and along the beautiful coastline, and when I reached the border safely, I couldn't have felt better. The most useful luggage brought from Japan is definitely a bike. However, it is a bit difficult to carry a bike from Japan, so if you spend 6 months in Los Angeles, I recommend you to buy it locally.

The second is regarding a club activity at UCLA. I belonged to JPAM (Japan-America Language & Culture Club) in the fall and winter quarter. In the club, several Japanese students who want to learn English and a large number of students who want to speak Japanese can meet and interact weekly after school. At the beginning of this JUACEP program, I felt that I had fewer opportunities to use English than other JUACEP members because the number of students in my laboratory was less, and my housemates were Japanese. So, I decided to join this club to improve my English skill. I could participate in dinners after club activities and drinking parties on weekends. As a result, I got many foreign friends as well as improving my English skill by this club. I made an appointment to meet one of foreign friends when he comes to Japan this winter, and I'm looking forward to it.



My life in the United States for half a year was not only fun as described above, but it was also difficult due to lack of my English skill, differences in culture and customs. However, these events were all irreplaceable and led me to my own growth. I would like to thank all of the people who supported me.



Findings through JUACEP

Name: Takaaki Miyachi

Affiliation at Nagoya University: Department of Micro-Nano Mechanical Science and Engineering

Participated program: Medium course 2019

Research theme: Finite Element Analysis of Contact in Asperities

Advisor at the visiting university: Prof. Shaker A. Meguid

Affiliation at visiting university: Department of Mechanical and Industrial Engineering, University of Toronto



I got many experiences through visiting Canada. The all experiences made me happy and grow. The first one is studying in University of Toronto. I had studied Finite Element Method (FEM) for six months. I did not have enough skills and knowledge about FEM at first. However, my professor gave me a textbook about FEM and my laboratory members helped me a lot how to use ANSYS. Actually, I wanted to stay more to learn FEM and obtain good discussion skills. Anyways, it greatly helped me to understand FEM. I really thank to those people and JUACEP program. Those experiences should have good effect for my career after I come back to Japan.

My life in Canada was so nice. I had stayed in homestay. My host family was so kind and gave me 2 meals every day. They had some homestay members like me. I could improve my English skills with them through chatting because they were English learner. Moreover, I went to a language school for 10 weeks in the morning. I could learn English a lot and make some friends there.

There are a lot of nature and big park in Canada. I enjoyed some outdoor activities. In autumn, I went to a big national park. Leaves change their color like in Japan. The view was so beautiful. In winter, I skied and did ice skating. It was so cold but nice experiences.



I joined the kendo club in University of Toronto. I have practiced kendo since I was 8 years old. I was really looking forward to playing kendo in Canada. I practiced kendo twice or three times in a week. It was difficult to tell about kendo in English. However, it was very interesting to learn how to explain about kendo techniques in English. My target was to join a kendo competition and win. I could not win the competition. But it was a good memory. Every kendo member was so kind and friendly to me. I really love them.

Finally, I really appreciate JUACEP program and all people who supported me.



Unforgettable life in UCLA

Name: Masahiro Itoh

Affiliation at Nagoya University: Aerospace Engineering

Participated program: Long course 2019

Research theme: The wind tunnel experiment of low profile double floating-elements shear stress sensor

Advisor at the visiting university: Prof. Chang-Jin Kim

Affiliation at visiting university: Department of Mechanical and aerospace engineering, University of California, Los Angeles



A life in UCLA is pretty valuable experience. I researched the sensor used in wind tunnel at Micro and Nano Manufacturing Laboratory in UCLA as a collaboration with fluid dynamics laboratory in Nagoya University I belong to. When I applied JUACEP program, I set a goal to be a person who has internationality. Here, internationality means the ability of communication without any language barrier. When I first started researching in the lab, I couldn't express my thoughts well. But by talking to my labmates actively and doing presentation every week, the ability of conveying my thoughts had pretty improved through eight months. Also, I understood how I should think in science field.

I met many excellent students in UCLA. They are energetic, smart, polite and hard worker. They changed my thoughts. By talking with and knowing them, I realized that struggles I have had is not a big deal. They told me I can put all my effort in the future.

I often went to lunch with labmates in the dining hall of hospital and eat healthy food. For dinner, I often went to dinning hall for UCLA students and restaurant with labmates. UCLA is located in urban area, so we can eat good, various kinds of food. I usually spent weekends traveling with friends. I visited Texas, New York, Alaska, Boston, Las Vegas, some national parks and so on. Each place has different character and worth to visit. Driving in vast extent of land is very exciting. Los Angeles is good place to live for me. It's sunny and warm almost every day and has a lot of place worth to visit.

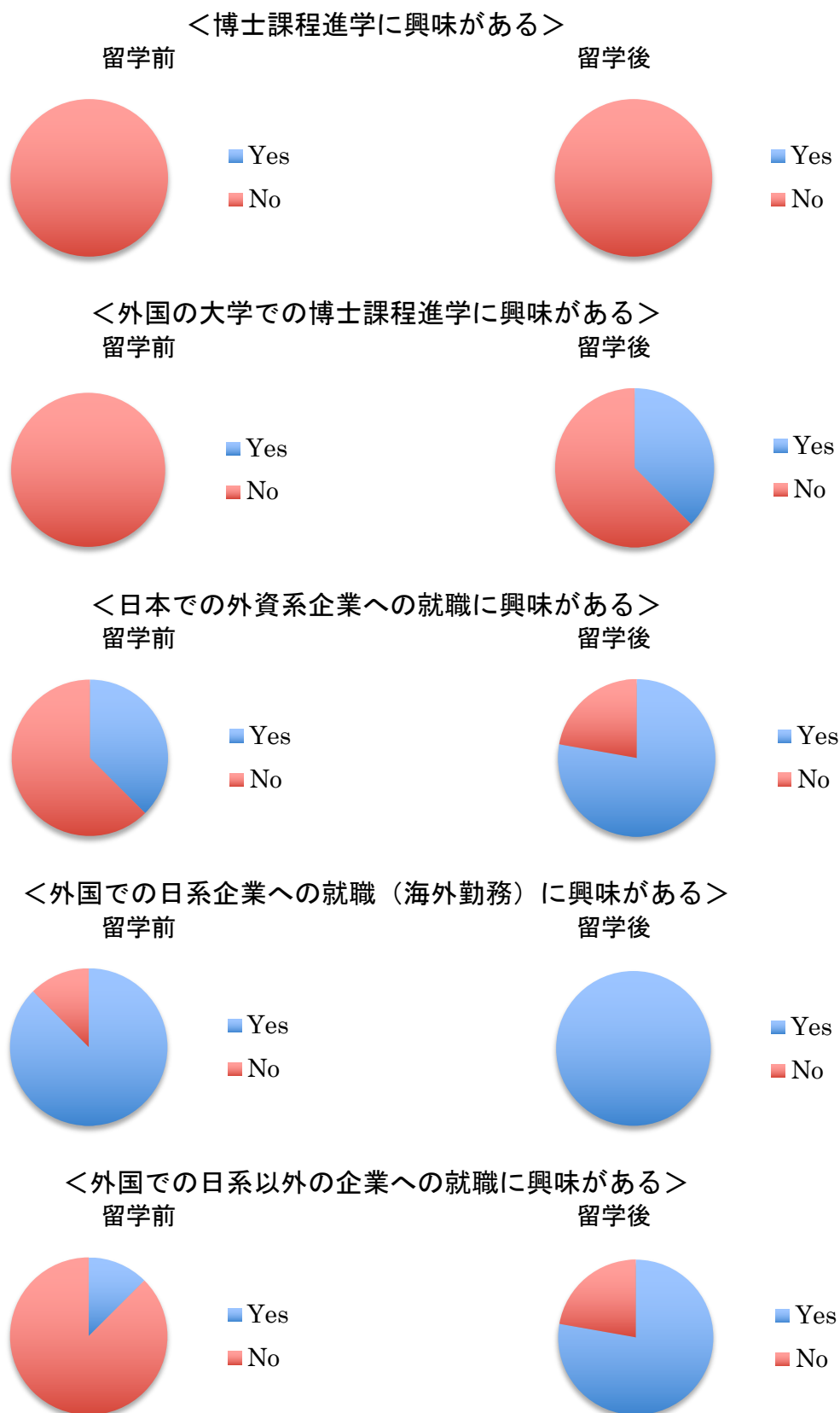
The one thing I'm regretting is about my roommate. The first three weeks, I lived with another JUACEP student. After these three weeks, I moved to another apartment because I planned to live with foreigner in order to improve my English communication skills. When I met new roommate first time, I felt he is a nice person, so I contracted for remaining seven months in that time. But couple of days after, I realized I can't live with him. But I can't move out because I already contracted remaining seven month. I had a lot of trouble between him. If you plan to share room with someone, you have to be very picky. Otherwise you enjoy life is going to be ruined. Your roommate is very important for daily life.



The life in UCLA is unforgettable, best enjoyable experience in my life and will influences on my future career. I appreciate to everyone I met in US and JUACEP.



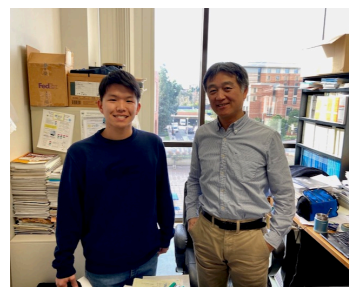
派遣プログラム参加者に行ったアンケート結果



アンケート結果まとめ 10年以上前から博士後期課程を目指す学生は国内で減少傾向だが、現地の研究チーム内で博士課程学生の役割・取組を目にして刺激を受け、外国での博士課程に興味を抱くようになる学生が毎年いる。また帰国後に外資系企業への就職や海外勤務に関心を持つようになることがアンケートで読み取れる。

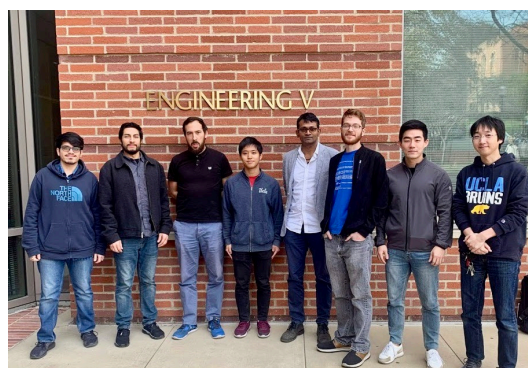
1. このプログラムの良かった点

- ・ 行きたい大学、学びたい研究室を自分で決められる。
- ・ 留学期間を自分で選べる。
- ・ 派遣先大学で必須の講義がないので、研究に多くの時間を割ける。
- ・ 世界最先端御技術を学べた。
- ・ アメリカの大学の研究チームの一員として参加するので日本との違いを知ることができ、日本の大学の研究室体系の良い点、悪い点を考えることができた。肌で感じたことを今後の研究に生かせると思った。
- ・ 受入先教授、家探しなど自分でやるため責任感が向上した。
- ・ 授業がないので平日は研究に集中し、休日にはアメリカを楽しむことができる。月10万円の給付型奨学金を受けられた。
- ・ アメリカでの就職フォーラムに参加できるので、日本にいるより就活を先駆けて体験できる。
- ・ 応募要件にTOEFLやIELTSが必須でなくTOEICの点数でも認められるので、応募時のハードルが低い。
- ・ 宿舎を自分で探すなど自由度が高く、いつかまた海外生活をするところがあるなら良い経験となる。



2. このプログラムで改善してほしい点

- ・ 改善して欲しい点は特にない。
- ・ 可能ならば JUACEP 用の寮などが準備されているとよい。宿舎探しは大変。家賃や物価が高いので奨学金だけでは足りないことがあった。
- ・ 家賃は安く見積もっても月 US\$800。奨学金 10 万円だけでは生活は無理。
- ・ 個人的にはもっと長く滞在したかったが就活があるから仕方がない、終了時期が就活と重ならないようなプログラムができるといい。
- ・ 事前の手続き、家探しなどは出発前に不安だったので、同じ派遣メンバーや過去の派遣者との交流の場があればよかった。(事務局より：交流のチャンスは毎年用意されています)



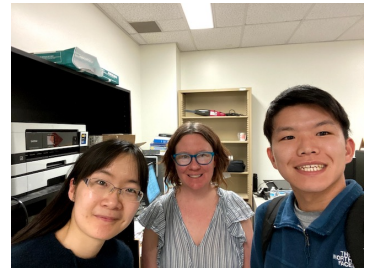
3. 住居について (A: 宿舎の見つけ方, 宿舎形態, 家賃, 大学までの足 B: 感想)

- ・ A:最初の1ヶ月は Airbnb で予約して出発し、その間に Craigslist で残りの月数の宿舎を見つけた。シェアハウスでプライベートルーム, US\$900/月, 自転車で 35 分。
B: 不安も大きかったが自分で探して交渉したことはいい経験だった。
- ・ A: Airbnb, vivinavi を利用した。ルームシェアで US\$1,000/月, 自転車で 30~45 分。
B: UCLA 近辺~サンタモニカ, ベニスあたりは治安が良く過ごしやすいかった。Craigslist でも探したが、偽の情報も多いい物件は見つけれなかった。
- ・ A: インターネットで探したホームステイ。朝食と昼食付きで CA\$825/月, バスと地下鉄で 60 分。
B: ホームステイは基本的に大学やダウンタウンから少し離れた場所となるが、家賃はそれほど高くなく、食事も提供され洗



濯もしてもらった。

- A : Craigslist, US\$1,000/月, 自転車約 20 分。
B : Craigslist は詐欺も多いので、極力事前にお金は払わない方がいい。万一デポジットを要求された場合は、払う前にテレビ電話などで家の中を案内してもらってからにすることを薦める。私はテレビ電話で家の中外を見せてもらった後 Google Map で二重チェックした。
- A : Craigslist, vivivnavi, Facebook を利用。アパートの一件を 3 人でシェア, US\$950/月+コインランドリー, 自転車約 20 分。
B : ルームメイトの 2 人が料理を全くしなかったのでキッチンを独占できた。物価が高いロスで毎日外食は大変なのでこれはありがたかった。また運良くマスタールーム (プライベートルーム+プライベートバスルーム) だったので、生活はしやすかった。ただ同じ家に他人が住んでいるという、日本ではあまりない状況なので、音を立てないようにしたり掃除当番を決めたりなど最後まで気を遣い、最大限のリラックスができなかった。
- A : 最初の 1 ヶ月は Airbnb で予約して出発し、その間に Craigslist で残りの月数の宿舎を見つけた。ホストファミリーの家の一室, US\$1,400/月, バスで 30 分。
- A : Airbnb, Craigslist を利用, US\$845/月, 徒歩 15 分。
B : Airbnb で最初の 3 週間分を予約して出発したが、最後の週になっても次の宿舎を見つけていなかったで焦っていた。安さと大学からの近さで選んだ Studio と呼ばれるタイプの間仕切りのない一部屋を 60 代男性とシェアする契約をした。相性が合わなかったが、留学終了までの契約をしてしまったため引っ越すことができなかった。家賃や契約書に関してのトラブルは取り返しのつかないことになり得るので、契約書類などはよく読み、家賃の支払い時は録画や録音で証拠を残しておくことよい。ルームメイトとの契約ではなくアパートと契約しておけば、ルームメイトとうまくいかなくなった時部屋を変わる可能性もある。ルームメイトは時間をかけても慎重に選ぶべきである。知人の中国留学生は、UCLA 内の中国人向け SNS を通じて US\$500/月のシェアルームを見つけた。中国人の友人がいれば頼んで見つけてもらうことも可能である。
- A : Airbnb で最初の 1 ヶ月を予約して出発、いい宿だったので 6 ヶ月に延長した。共有スペースのリビング・キッチンに、二人用の寝室が二つある (計 4 人収容) の家, US\$1,070/月, 徒歩 25 分。
B : ルームメイトはペルー人, イタリア人, フランス人という多様性で、皆優しく気のいい人ばかりだったので、英語での会話の機会が多いということ以外にもいいことづくめだった。恐れずシェアルーム形態にすることをお薦めする。



4. 滞在中の印象深いことなど

- 一番の思い出は剣道部に入部したこと。剣道を通じてたくさんの友達を作りたくさんの経験をした。JUACEP で留学する人にはクラブに参加することを大いに勧めたい。
- 外国人とのハウスシェアは良い経験になった。
- グループミーティングで学生も積極的に発言しているのを見て、日本にはあまりないアメリカらしさを感じた。
- 言語、研究、人間関係などどんなことでも自身の積極性が大切だと身をもって体感した。
- ロストバゲッジの荷物が留学初日に戻ってきたこと。
- 夏のロサンゼルスは、朝晩が意外と寒いこと。たとえば 1 月でも昼間は暖かく水着でビーチバレーができること。
- UCLA の英語日本語交流クラブに入れたこと。
- 日本の研究室の方が実験装置の数が豊富だと感じた。
- 自転車でロサンゼルスからメキシコへ行ったこと。



- アメリカでは、基本的にフレンドリーで優しい人が多い。でも観光地などでは、親しげに近づいてきた人にまじめに対応しているとお金を要求されたりするので要注意。
- 研究チームのメンバーとヨセミテ国立公園に行ったこと。
- 11月にグランドキャニオンに行こうとしたら、異例の雪で結局辿り着けず、さらに帰途、雪で横転したトラックのために9時間足止めを食らった。進むことも戻ることもできず車内でゲームで時間を潰した。西部の人はスタッドレスタイヤを付ける習慣がないのか（そもそもレンタカーにスタッドレスタイヤのオプションがない）、雪が降るたびに道路が通行止めになる。車での旅行を確実にしたいなら、夏がおすすめ。



- 高価な自転車を盗まれた友人がいる。物の管理には日本にいるときより十分気を付けなければいけない。
- 留学するまでは、PhD学生として給料をもらいながら研究を行うという選択肢があることさえ知らず、日本においてはその道を選ぶ人はかなりの少数派で情報も多くない。留学したことで視野が広がり、今後のキャリアを考える上で素晴らしい経験になった。
- ロスでの生活が始まってすぐ、シェアルームのメンバーで顔合わせの食事会をした。外国人の学生と食事をする機会がなかったこと、まだ英語能力が低く流暢に会話できず悔しい思いをした。必ず留学中に英語能力を鍛えて対等に会話できるようにすると誓った出来事だった。この日をきっかけに積極的に会話することを心がけ、徐々に世間話をしたり、映画に出かけたりして、本当の意味で打ち解けることができた。



5. その他、自由コメント

- 手厚いサポートのおかげで、よい留学生活を過ごすことができました、ありがとうございました。
- 人生で最も濃い半年間を過ごせたと確信している。出発前からのサポートをありがとうございました。
- 初めて親元を離れて暮らす場所がロサンゼルスで最初は不安だったが、予想より不便もなく快適に過ごすことができました。
- いろんな面でとてもいい経験ができました。プログラムに本当に感謝しています。
- 行く前は緊張していたが、行ってみると新鮮なことの連続で半年間があっという間だった。留学を許可してくれた先生、両親、資金の支援をしてくれた祖父母、東山会、JUACEPの方々にとっても感謝しています。



Copyright © JUACEP 2020 All Rights Reserved

Published in June 2020

Japan-US-Canada Advanced Collaborative Education Program (JUACEP)

Graduate School of Engineering

Nagoya University

Furo-cho, Chikusa-ku, Nagoya 464-8603, Japan

JUACEP@engg.nagoya-u.ac.jp

<http://www.juacep.engg.nagoya-u.ac.jp>